R. & M. No. 2886
(15,083)
A.R.C. Technical Report

MINISTRY OF SUPPLY

AERONAUTICAL RESEARCH COUNCIL
REPORTS AND MEMORANDA

Pressure and Boundary-layer Measurements on a Two-dimensional Wing at Low Speed

By

G. G. BREBNER, M.A., and J. A. BAGLEY, B.Sc.

LONDON: HER MAJESTY'S STATIONERY OFFICE
1956
PRICE 12*s* 6*d* NET

Pressure and Boundary-layer Measurements on a Two-dimensional Wing at Low Speed

By

G. G. BREBNER, M.A., and J. A. BAGLEY, B.Sc.

COMMUNICATED BY THE PRINCIPAL DIRECTOR OF SCIENTIFIC RESEARCH (AIR), MINISTRY OF SUPPLY

Reports and Memoranda No. 2886*

February, 1952

Summary.—Results are given of pressure measurements and boundary-layer traverses on a two-dimensional wing with 10 per cent RAE 101 section at Reynolds numbers of $1{\cdot}6 \times 10^6$ and $3{\cdot}2 \times 10^6$. These results, which have been integrated to give lift, drag and aerodynamic-centre characteristics, are used to check some calculation methods for the growth of the turbulent boundary layer and for the effect of a known boundary layer on the pressure distribution.

It is concluded that the calculation of the boundary layer still needs a little refinement before it is accurate enough to predict viscosity effects on pressure distribution, lift, drag and aerodynamic centre ; but that these effects can be calculated if the actual boundary-layer characteristics are known.

1. *Introduction.*—This note is a further contribution to the study of viscous flow about a two-dimensional aerofoil. The effect of viscosity is not only to produce a drag force due to the shear stresses on the aerofoil surface—skin friction—but also to modify the pressure distribution over the aerofoil. This brings about a reduction in lift, a change in the aerodynamic centre, and another drag force, the form drag. Primarily the viscosity ensures that the flow leaves the trailing edge smoothly, and in the limiting case of zero viscosity it causes the rear stagnation point to be at the trailing edge (Kutta–Joukowski condition). Hence it is responsible for the lift force. However, the fact that the boundary layer is, in general, thicker on the upper surface than on the lower surface means that the dividing streamline in the wake seems to spring from a point on the upper surface, and the lift is thus somewhat reduced. Work done on this problem has been summarised by Betz in *Aerodynamic Theory* (edited by Durand) Vol. IV, and more recently by Preston[1], whose analysis forms the basis of the present treatment.

We present here some new experimental data on a two-dimensional wing having a symmetrical profile (RAE 101, thickness/chord ratio 10 per cent). The investigation was prompted by a swept-wing calculation in which the need for information on the two-dimensional lift slope became apparent[2]. The data have been analysed to see how far recent theoretical investigations enable viscosity effects to be predicted from the given aerofoil shape only. No attempt has been made to confirm empirical rules for the effects on lift, drag and pitching moment. Instead, a method has been investigated for calculating the effects on the pressure distribution of a boundary layer whose characteristics are known. Methods of calculating the growth of the boundary layer have also been studied. Accordingly, the experiments comprise both boundary-layer and pressure measurements.

* R.A.E. Report Aero. 2455, received 23rd July, 1952.

The conclusion is reached that the methods of predicting the growth of the boundary layer are sound in themselves but are handicapped by insufficient initial data about conditions in the transition region and near the trailing edge. It is therefore not yet possible to predict the boundary layer with sufficient accuracy for calculating the modification by viscosity of the pressure distribution over the aerofoil surface.

When the boundary layer is known, however, *e.g.*, from experiments, the method for calculating the viscosity effects predicts the lift with good accuracy and the centre of pressure with sufficient accuracy for practical purposes. It is not yet good enough for estimating the form drag, but this is not the primary purpose of the method.

2. *Details of Model and Tests.*—The tests were done in the No. 2, $11\frac{1}{2}$-ft $\times$ $8\frac{1}{2}$-ft Wind Tunnel at the Royal Aircraft Establishment in February, March and June, 1951. The model was a two-dimensional unswept wing of 30-in. chord spanning the shorter dimension of the tunnel. The profile section was RAE 101, thickness/chord ratio 10 per cent. In Ref. 2, loading calculations on a series of wings of 45 deg sweepback with profile section RAE 101, thickness/chord ratio 12 per cent, included a factor to the two-dimensional lift slope at $C_L = 0$ to take account of the initial loss of lift due to the boundary layer (which at low C_L has not yet begun to flow outwards). The thickness and profile shape of the present two-dimensional wing were chosen to give approximately the same pressure distribution as the 45 deg swept wing at a C_L of about 0·3. The value of the factor used in Ref. 2 could thus be checked.

The wing was made of wood with a Tufnol trailing edge, and the section was accurate to within 0·0003c, *i.e.*, 0·01-in. Pressure measurements on the wing surface were made by means of two rows of flush holes, 4-in. apart, at the centre of the span. The holes had a diameter of $\frac{1}{32}$-in. and their chordwise positions on the two rows were staggered. Thus 26 chordwise measuring points were available on each surface without over-crowding the pressure holes and unduly roughening the surface. The pressure tubes were led out at the ends of the wing (which were outside the tunnel) to the multitube manometers on which the pressures were read.

The boundary layer at the section midway between the rows of pressure holes was traversed perpendicular to the chord-line by a pitot-tube mounted on a gantry. A sketch of the apparatus is given in Fig. 21. The supporting structure can have no effect on the total-head measurement by the pitot-tube, and it was far enough from the section being measured to have no appreciable effect on the velocity. Any such error in velocity is certainly less than 0·5 per cent. This is within the accuracy of the surface pressure measurements and is no worse than the error involved in the assumption that p is constant through the boundary layer. Also it is too small to have a noticeable effect on the boundary-layer thickness. The interference from the stem of the pitot-tube is much less than that from the gantry. The traversing mechanism was electrically driven and the distance of the pitot from the wing surface could be read to within 0·0004-in. The pitot-tube had a flattened square-cut nose, 0·02-in. deep and 0·04-in. wide. The centre of the tube could therefore not approach nearer to the wing than 0·0003c. The uncertainty in the zero reading at the wing surface was about $\pm$ 0·001-in., *i.e.*, $\pm$ 0·00003c. The pitot pressures were read on a Prandtl type micro-manometer, and could be read to 0·05 mm alcohol. In the present tests this represented less than 0·001q_0.

The tests consisted of pressure measurements and boundary-layer traverses. The former were made at speeds of 100 f.p.s. and 200 f.p.s., giving Reynolds numbers based on the wing chord of $1{\cdot}6 \times 10^6$ and $3{\cdot}2 \times 10^6$ respectively. The incidence range extended beyond the stall at the lower speed and up to 8·19 deg at the higher speed, boundary-layer transition being allowed to occur freely. Further tests were made at both speeds with transition fixed at 0·15c on one or both surfaces. On all these runs the liquid-film evaporation technique[3] was used to indicate the position of transition. Transition was fixed when required by a wire 0·018-in. in diameter, attached to the wing by cellulose tape.

The boundary-layer tests consisted of pitot traverses perpendicular to the chord-line at incidences of 0 deg, $\pm$ 4 deg and $\pm$ 8 deg, and at various chordwise positions between $0{\cdot}30c$ and the trailing edge. Transition was not fixed for these tests, the transition position being checked by liquid evaporation before each traverse.

The incidence in all these tests was measured by the movement of a light beam which was reflected from a small mirror countersunk in the wing surface well clear of the pressure holes. The size of the scale and the sensitivity of the system allowed the incidence to be read to about $0{\cdot}01$ deg. Zero incidence was found by adjusting the wing until the pressures on both sides were equal. A small amount of wing twist, due to the aerodynamic load and proportional to incidence, was detected and measured. At $R = 1{\cdot}6 \times 10^6$, the angle of twist $\Delta\alpha = 0{\cdot}004\alpha$, and at $R = 3{\cdot}2 \times 10^6$, $\Delta\alpha = 0{\cdot}02\alpha$. The angles of incidence quoted in the results have been corrected for this twist, as well as for the usual tunnel constraint. The latter is given by $\Delta\alpha \text{ deg} = 0{\cdot}0284c^2C_L = 0{\cdot}1774C_L$.

3. *Results and Discussion.*—3.1. *Pressure Measurements.*—The results of the pressure measurements are given in Tables 1 and 2 and in Figs. 1 to 8. Figs. 1 and 2 show the development with incidence of the chordwise pressure distribution at the lower Reynolds number of $1{\cdot}6 = 10^6$ with transition occurring freely. They extend up to $\alpha = 10{\cdot}22$ deg at which point the flow has not yet broken down. There were not enough pressure holes near the nose to define the suction peaks accurately at incidences greater than 4 deg. In Ref. 4 pressure-plotting experiments show the existence of laminar separation near the nose of an aerofoil at incidences above about 4 deg. The separated flow reattaches very quickly at first, forming a small ' bubble.' At the stall the flow fails to reattach and breaks down over the whole chord. In the present tests the pressure measurements show this effect at incidences greater than 6 deg, although the holes are too widely spaced to define the separated region accurately. The separation ' bubble ' is too far forward to appear in Figs. 1 and 2. Fig. 3 shows that the flow broke down between $\alpha = 10{\cdot}7$ deg and $\alpha = 11{\cdot}2$ deg.

Fig. 4 compares the measured pressure distribution at zero incidence, for free transition and at both Reynolds numbers, with the potential flow distribution calculated by the method of Ref. 5. The experimental points plotted are the mean values for the upper and lower surfaces. The agreement between experiment and the solution for a perfect fluid is very good, especially ahead of the measured transition point. The apparent scale effect near the peak suction is a compressibility effect, which is allowed for in the calculations. The only marked discrepancy between theory and experiment is in the last 1 to 2 per cent of the chord. At the trailing edge there is a stagnation point in potential flow, i.e., $C_p = +1{\cdot}0$. The measured value is about $+0{\cdot}16$ (Tables 1 and 2). The discrepancy is due to the very steep pressure gradient over the last few per cent of the chord which thickens the boundary layer and increases the effect of viscosity on the pressure distribution.

Fig. 4 also shows that in a region around the measured transition position the pressure is slightly increased compared with the theoretical value, *i.e.*, there is a reduction in velocity. This could be connected with the change in displacement thickness which occurs at transition.

Figs. 5 to 7 illustrate the effect at small incidences of fixing transition artificially at $0{\cdot}15c$ on one or both surfaces at the higher Reynolds number of $3{\cdot}2 \times 10^6$. Figs. 5 and 6 show the upper and lower surface pressures at zero incidence. In the former, two sets of points refer to free transition, and in the latter, two sets refer to fixed transition. The points of each pair will not be expected to coincide exactly, however, as one case is symmetrical about the chord-line (transition free or fixed on both sides) and the other is asymmetrical (transition fixed on one side only). There will thus be a small difference in the circulation round the aerofoil in the two cases and a corresponding difference in the pressure distribution. This is shown by the measurements. In Fig. 5 the asymmetrical points are slightly more negative than the corresponding symmetrical ones (free transition on both sides). In Fig. 6 the asymmetrical points are less negative than

the corresponding symmetrical ones (transition fixed on both sides). In Fig. 5 the doubtful measurement of the upper surface pressure at $x/c = 0{\cdot}20$ has been included as it still shows consistently the effect of fixing transition, which is to shift the ' dip ' in the pressure distribution from the free transition point to the fixed one. The effect also shows up in Fig. 6 though it is not so clear-cut as in Fig. 5. The size of the dip appears to be about the same for free and artificially induced transition so that fixing transition would not lead to any marked systematic effect on the lift (*see* also section 5).

The region in which the pressures are affected by transition is about $0{\cdot}25c$ in length. It would appear from Figs. 4, 5 and 6 that the transition point indicated by the liquid-film evaporation method lies about 25 to 30 per cent along this region.

The above features are again present in the pressure distributions at $\alpha = 2$ deg (Fig. 7). On the lower surface the effect of transition on the pressure distribution is more widespread. The small asymmetry effect on the circulation is still noticeable. At incidences above 3 deg, the observed transition point is further forward than $0{\cdot}15c$ on the upper surface, and so no transition effect should be obtained, except possibly a very small one due to the asymmetry already mentioned and another one due to increased boundary-layer thickness on the lower surface (*see* also section 5).

It is worth noting that transition occurs well behind the peak suction. This is shown not only in Figs. 4 to 7 but also by comparing the transition points plotted in Fig. 8 with the pressure distributions in Figs. 1 and 2. In boundary-layer calculations it is sometimes recommended that transition be assumed to take place just after the peak suction. For aerofoils with pressure gradients similar to RAE 101 section at $R \leqslant 3 \times 10^6$, this estimate would appear to be too far forward.

3.2. *Lift, Drag and Pitching Moment.*—By graphical integration of the measured pressure distributions, the normal and tangential force coefficients, C_N and C_T, were obtained, and hence C_L, C_D and h/c. These quantities are tabulated in Tables 3 and 4 and plotted against C_L in Figs. 10 to 12. The coefficients in Table III are mean values between positive and negative incidences. The mean variation in C_N and C_L is $0{\cdot}003$ and in C_T and C_D is $0{\cdot}0008$.

The term ' two-dimensional lift slope ' (a_0) at any incidence α_1, is here defined as $[C_L/\alpha]_{\alpha=\alpha_1}$ and not as $[\partial C_L/\partial\alpha]_{\alpha=\alpha_1}$. This is done for two reasons. Firstly, the ratio C_L/α is more useful than $\partial C_L/\partial\alpha$ for calculation purposes, since C_L may be immediately obtained as the product of the lift slope and the incidence. Secondly, the slope of the lift curve at any point is hard to determine exactly and, in practice, the lift slope quoted is usually obtained by some averaging process over a certain C_L range, *e.g.*, $0 \leqslant C_L \leqslant 0{\cdot}6$. In Fig. 10 the experimental lift slopes according to the above definition are plotted against C_L, and a value obtained by a typical averaging process over the range $0 \leqslant C_L \leqslant 0{\cdot}6$ is shown by a dotted line. The latter value is smaller at $C_L = 0$ and is, of course, constant over the range which defines it.

All the experimental lift slopes are based on the incidence measured from zero lift, which, for the symmetrical wing, was the same as the geometric incidence. With a transition wire fitted on one side only, zero lift was no longer at the geometric zero, due to the extra circulation set up by the asymmetry. The C_L at zero incidence was $+ 0{\cdot}011$.

$(a_0)_T$, the two-dimensional lift slope in a perfect non-viscous fluid, was obtained from Ref. 6 and is in accordance with the rough rule for a thick profile $(a_0)_T = 2\pi\{1 + (0{\cdot}8 \times t/c)/(\cos\phi)\}$ where ϕ is the sweep angle, if any. In this case $(a_0)_T = 6{\cdot}793$ at all values of C_L.

In Fig. 10 $(a_0)/(a_0)_T$ is plotted against C_L for both values of R and all transition conditions. In the upper diagram the full C_L range to the stall is covered for the free transition case, and the lift slope is seen to decrease in an approximately linear manner as C_L increases. This decrease is a measure of the viscosity effects which increase with C_L because of the thickening of the boundary layer. Even at zero lift the boundary layer reduces the lift slope well below the non-viscous potential flow value. In this case $(a_0)/(a_0)_T \simeq 0{\cdot}92$. (The calculated lift slopes will be discussed in section 5.)

The middle diagram of Fig. 10 compares the lift slopes at the two Reynolds numbers. The scale effect is small. The lift slope decreases rather more slowly at the higher R, since the boundary layer thickens more slowly.

The lift slopes with different transition conditions may be compared in the upper and lower diagrams of Fig. 10. Rather surprisingly, no consistent effect is apparent. The slight increase of lift, with transition fixed, at $R = 1{\cdot}6 \times 10^6$ is not reproduced at $R = 3{\cdot}2 \times 10^6$. It has already been noted in Figs. 4 to 7 that the ' dip ' in the pressure distribution near the transition region is merely displaced when transition is fixed, and the net effect on the chordwise integral is not noticeable.

Figs. 11 and 12 show similar comparisons of the drag and aerodynamic centre. The form drag, C_D, is plotted against C_L in Fig. 11. The steep rise of C_D at the higher values of C_L shows that C_D increases more quickly than C_L^2 and that a quadratic law is therefore not appropriate for the form drag of this section. The top and bottom diagrams show no systematic difference between fixed transition and free transition conditions, except possibly at $R = 3{\cdot}2 \times 10^6$ where fixing transition seems to cause a slight increase in form drag. The scale effect is large, as shown in the middle diagram, C_D at $R = 3{\cdot}2 \times 10^6$ being only about 50 to 60 per cent of that at $R = 1{\cdot}6 \times 10^6$.

There is no scale effect on the aerodynamic centre (Fig. 12). Fixing transition seems to cause a slight rearward movement at $R = 1{\cdot}6 \times 10^6$, but this is not apparent at the higher R.

3.3. *Boundary-layer Measurements.*—The velocities and total pressures in the two-dimensional boundary layer are tabulated in Table 7, the static pressure at the trailing edge in Table 8, and the displacement thickness, δ^*, the momentum thickness, θ, and the form parameter δ^*/θ in Table 9. The results are illustrated in Figs. 13 to 17. δ^* and θ were obtained by graphical evaluation of the integrals :

$$\int_0^{\delta^*} \frac{V_p}{V_0}\,dz = \int_0^{\delta} \left(\frac{V_p}{V_0} - \frac{V}{V_0}\right) dz, \qquad \text{(Ref. 1)}$$

and

$$\theta = \int_0^{\delta} \frac{V}{V_0}\left(1 - \frac{V}{V_0}\right) dz,$$

where V_p is the velocity about the aerofoil surface in a perfect non-viscous fluid. All boundary-layer measurements were made at a Reynolds number of $1{\cdot}6 \times 10^6$; the figures quoted for the lower surface were actually obtained by setting the wing at negative incidence.

Figs. 13 to 15 show velocity and total-head profiles at various incidences and chordwise positions. The total head was measured directly by the pitot-tube and the velocity found by subtracting from the total head the measured static pressure on the surface. At the trailing edge the static pressure was obtained from a wake traverse (*see* Table 8) but this is liable to error since the direction of the streamlines at the trailing edge is not known. The results have not been corrected for the displacement of the effective centre of the pitot-tube due to the transverse pressure gradient. Since this investigation is primarily concerned with the effect of the boundary layer on lift, a detailed analysis of the velocity profiles has not been made. Figs. 13 to 15 show that on the upper surface the total-head profile at the trailing edge is considerably different from those at other chordwise positions. This is due to the change in pressure through the boundary layer becoming appreciable near the trailing edge.

Since the trailing-edge traverse was done just behind the wing (within 0·05-in., *i.e.*, $0{\cdot}0015c$), the experimental value of the displacement thickness may be slightly lower than at the actual trailing edge, since δ^* decreases quickly behind the wing.

Figs. 16 and 17 show the variation of δ^* and θ with incidence and chordwise position. In these figures, negative values of α correspond to lower-surface conditions at positive α. δ^* and θ vary in a similar way with x/c. Near the trailing edge on the upper surface at positive incidences δ^* increases more rapidly than θ, thus causing the characteristic rise in the form parameter in a high adverse pressure gradient. This is less pronounced at 4·09 deg than at 8·18 deg where the value of δ^*/θ at the trailing edge is just below the critical range for separation to occur, namely $2{\cdot}0 < \delta^*/\theta < 2{\cdot}8$. It therefore seems possible that, above 8 deg, the flow may be just starting to separate near the trailing edge. This would not be sufficiently widespread to show up in the pressure distributions of Fig. 1. Any such separation at the trailing edge however would be unlikely to affect $C_{L\,\max}$, since the latter is here determined by laminar separation near the nose without reattachment (section 3.1).

Figs. 16 and 17 also show δ^* and θ plotted against α, the variation of the two quantities being again similar. The effect of incidence is small at negative angles compared with that at positive angles.

4. *Theoretical Prediction of the Boundary Layer.*—The ultimate aim of boundary-layer investigations is to be able to predict, from the aerofoil shape only, the effects of viscosity on aerodynamic characteristics such as lift, drag and pitching moment at any given Reynolds number. Even in the simplest case, that of the two-dimensional aerofoil, this is not yet possible. Two requirements are necessary, a method of calculating the growth of the boundary layer—laminar or turbulent—over the aerofoil, and a method of calculating the influence of this boundary layer on the pressure distribution. It will be shown in section 5 that the second of these operations can now be adequately performed, at least as far as lift and pitching moment are concerned, by calculating the pressure distribution in potential flow over a hypothetical aerofoil whose shape depends on the displacement thickness.

The calculation of the boundary-layer characteristics, however, does not yet seem to be possible with sufficient accuracy. Methods exist for approximate prediction of both the laminar and turbulent regions. For present purposes the latter is usually much more important. The methods of Refs. 7 and 8 for calculating δ^* and θ in a turbulent boundary layer were found to predict their growth with good accuracy between transition and the trailing edge as long as the velocity distribution is accurately known. The actual values of δ^* and θ are sensitive to the initial conditions at transition. The conditions in the transition region are not yet well established, and errors in δ^* (obtained as the product of δ^*/θ and θ) of the order of 10 to 20 per cent may occur through this uncertainty. The actual position of the transition region can only be forecast within rather wide limits.

A more serious error may arise from the interdependence of the boundary layer and the velocity distribution. For practical purposes the initial velocity distribution should be accurate enough to give good boundary-layer results without resorting to a lengthy iteration process. Over most of the chord the potential-flow solution is satisfactory. At the trailing edge, however, this solution has a stagnation point for sections with a finite trailing-edge angle, whereas the true velocity is not much less than the free-stream value. This means that the boundary-layer calculations are very inaccurate near the trailing edge. Since δ^* will be used to determine an effective camber and change of incidence due to the boundary layer, the inaccuracies at the trailing edge cause large errors in the calculated viscosity effects. Thus the potential-flow velocity distribution is not a suitable starting point for a practical calculation, unless modified near the trailing edge.

Calculations of the growth of the boundary layer by the method of Ref. 7 were compared with the experimental data from the present tests for $\alpha = 4{\cdot}09$ deg. Two approximate velocity distributions were assumed near the trailing edge, with the following effect on the calculated δ^*.

	Potential flow	First approximation: potential flow to $x/c = 0{\cdot}99$; then smooth curve to $V/V_0 = 0{\cdot}866$ at T.E.	Second approximation: potential flow to $x/c = 0{\cdot}80$; then tangentially to $V/V_0 = 0{\cdot}96$ at T.E.
C_p at trailing edge	$+1{\cdot}0$	$+0{\cdot}250$	$+0{\cdot}078$
$\frac{\delta^* \text{ calculated}}{\delta^* \text{ experimental}}$	—	$2{\cdot}0$	$0{\cdot}85$

The measured C_p at the trailing edge at this incidence was about $+ 0{\cdot}14$, *i.e.*, between the two assumed values used in the calculation. This, if inserted in the method, would have made the calculated δ^* about the same as experiment. Thus the method seems to be satisfactory in itself provided (*a*) the initial values at transition are accurately established, and (*b*) a good approximation to the velocity distribution is available near the trailing edge.

5. *Calculation of the Viscosity Effect on the Pressure Distribution.*—As seen in section 4, theoretical methods of predicting the boundary layer on a given two-dimensional aerofoil are not yet sufficiently refined for purposes of calculating the lift, drag and pitching moment in viscous flow. In order to perform such viscous-flow calculations, therefore, use has to be made of experimental boundary-layer data. This has been done in the present case, and the calculated results have been compared with those from the pressure measurements. The calculated values of C_N, C_T, C_L, C_D and h/c are given in Table 5 and compared with experiment in Figs. 10 to 12 and 18 to 20.

At any point on the aerofoil the displacement thickness, δ^*, is considerably less than the boundary-layer thickness, δ, and represents approximately the amount by which the streamlines of non-viscous flow are displaced away from the aerofoil by the presence of the boundary layer. By assuming that such displacement takes place uniformly from the surface of the aerofoil, one can represent the real flow by the potential flow around a hypothetical aerofoil shape constructed by adding the appropriate δ^* to each point on the two surfaces. In the wake behind the trailing edge δ^* decreases until it reaches a final value (equal to θ) on each side of the dividing streamline. The potential flow should therefore be calculated for the complete profile built up round the original aerofoil and the dividing streamline. This dividing streamline would start from the ' trailing edge ' of the hypothetical aerofoil which, to start with, is arbitrarily assumed to be the midpoint between the upper and lower displacement thicknesses. According to Ref. 1, however, the circulation so obtained must subsequently be modified to satisfy the Taylor condition that equal amounts of positive and negative vorticity must be shed into the wake.

At any non-zero incidence δ^* will be different on the upper and lower surfaces of a symmetrical aerofoil. The new aerofoil will have its ' trailing edge ' displaced and will therefore have a camber and a change of effective incidence, $\Delta\alpha$, compared with the original section. At positive incidences δ^* is greater on the upper surface than the lower surface, the ' trailing edge ' is displaced upwards and the camber and $\Delta\alpha$ both act so as to reduce the lift below the value given by the potential flow solution for the original profile. If the latter is symmetrical, the curve of $\frac{1}{2}(\delta^*_{\text{U.S.}} - \delta^*_{\text{L.S.}})$ against x/c is the mean line of the hypothetical aerofoil. (Fig. 9).

In the present tests no measurements were made in the wake behind the wing. Therefore the new profile defined by δ^* is not known beyond $x/c = 1{\cdot}0$. The pressure was first calculated by the method of Ref. 5 over a profile made up of the original RAE 101 thickness distribution superimposed on the new mean line with camber and $\Delta\alpha$ due to the boundary layer. Although

the thickness effects are clearly going to be underestimated, this will only be appreciable near the trailing edge. Fig. 18 shows the experimental pressure distribution over the last 25 per cent of the chord at $\alpha = 8 \cdot 18$ deg compared with that obtained by the above calculation (curve (*a*)). Two other calculated curves are included in Fig. 18. These were attempts to allow for the true thickness of the new profile near the trailing edge. Both represent the pressure over a profile obtained by superimposing the measured δ^* on the RAE 101 profile. In the case of curve (*b*) this new profile was assumed to continue downstream with the same thickness as at the trailing edge. In the case of curve (*c*) the new profile was assumed to go discontinuously to zero at the trailing edge and to have no wake, and can therefore be calculated by the method of Ref. 5. Cases (*b*) and (*c*) thus differ by the presence of a strong isolated sink at the trailing edge. It can be seen in Fig. 18 that the effects are widely dissimilar, C_p at the trailing edge being between 0 and $1 \cdot 0$ on curve (*b*), and equal to $-\infty$ on curve (*c*). The correct answer lies somewhere between these two, since δ^* decreases behind the wing, eventually reaching a value equal to 0 on each side of the dividing streamline. Thus instead of the isolated sink at the trailing edge by which one goes from (*b*) to (*c*), a distribution of sinks over part of the dividing streamline is required. This distribution can only be determined when δ^* is known behind the wing, and this knowledge is therefore necessary for an accurate calculation of the pressure distribution.

Fig. 18 shows however that the difference of upper and lower surface pressures is almost the same for curves (*a*), (*b*) and (*c*), and so, for purposes of calculating the lift the method of curve (*a*) should be satisfactory. One would not expect the form drag to be adequately predicted since the errors in pressure near the trailing edge would add instead of cancelling each other. An accurate estimate of the form drag would require a solution for the true profile.

It has already been stated that initially the trailing edge of the hypothetical aerofoil is arbitrarily fixed midway between the upper and lower displacement thicknesses at $x/c = 1 \cdot 00$ and that fulfilment of the Taylor vorticity condition requires the circulation to be changed slightly from this initial value. This means a correction to the $\Delta\alpha$ term, the effect on the lift wing being represented by the K_2 factor of Ref. 1. This has been applied in the present calculations, the values of K_2 having been obtained by interpolation between those given in Ref. 1 for simple Joukowski and Piercy 1240 aerofoils.

Figs. 19 and 20 show a comparison between the experimental results and the calculated chordwise loadings. In Fig. 19 the loading at $\alpha = 4 \cdot 09$ deg is plotted in a conventional manner. In Fig. 20, $\Delta C_p \sqrt{(x/c)}$ is plotted against $\sqrt{(x/c)}$: this shows up more clearly the effects which contribute to the loss of lift. At $\alpha = 8 \cdot 18$ deg the effects of camber, change of effective incidence and K_2 are shown separately. As would be expected from the shape of the mean line (Fig. 8) the camber effect is most noticeable at the rear of the section, while the effect of $\Delta\alpha$ is a constant factor to ΔC_p along the chord. The final curve for the chordwise loading with boundary layer gives good agreement with experiment at $4 \cdot 09$ deg and $8 \cdot 18$ deg (Fig. 20).

It will be noticed that both at $4 \cdot 09$ deg and $8 \cdot 18$ deg there is a ' dip ' in the calculated loadings near the trailing edge. This deviates from the experimental results and may be partly due to the flow not following the sharply curved camber-line near the trailing edge. But even if it did follow the section shape, the curvature of the streamlines near the trailing edge would be so great that the condition for the static pressure to be constant through the boundary layer would not exist[1]. Therefore the static pressure calculated at the edge of the boundary layer (as is done here) would not be the true static pressure on the surface. The effect on the calculated C_N is very small, as can be seen by comparing the experimental and estimated results in Tables 3 and 5.

Referring back to Figs. 10 to 12, experimental values of the two-dimensional lift slope, form drag and pitching moment are compared with the calculated values for viscous flow derived from Fig. 20, *i.e.*, from experimental boundary-layer results. Since the boundary-layer data is available for only two values of C_L the calculated curve of $(a_0)/(a_0)_T$ against C_L (Fig. 10) has been drawn as a straight line passing through these points. This agrees well with the measured lift slopes and gives a value for $(a_0)/(a_0)_T$ at $C_L = 0$ of $0 \cdot 92$. This was the value used in Ref. 2 when calculating

the lift slope at zero lift of an infinite wing sheared by 45 deg. This had a RAE 101 section, 12 per cent thick, such that the pressure distribution was very similar to that of the present two-dimensional wing. At zero lift the spanwise flow in the boundary-layer characteristic of swept wings is not appreciable, and, in any case, is the same on both surfaces, so that the two-dimensional results may be confidently applied.

Fig. 10 shows that the calculation method is very good for estimating the lift. Fig. 11 shows that it is not good enough for estimating the form drag. The simplification in profile shape near the trailing edge causes too great an inaccuracy. The magnitude of C_D is so small that any useful calculation method must be very accurate, especially near the trailing edge. In view of the large scale effect shown in Fig. 11, however, it may be that at flight Reynolds numbers the form-drag error will be unimportant. In any case the form drag would, in practice, be calculated along with the skin friction by a method such as that of Refs. 9 and 10. For the present model this method gives profile-drag values of 0·0056 and 0·0062 for the 10 per cent thick sections of Refs. 9 and 10 respectively. The experimental value of the profile drag, obtained from the boundary-layer traverse just behind the trailing edge by the methods of Jones and Betz, is 0·0059.

The effect of the error at the trailing edge is also apparent in Fig. 12, where the aerodynamic centre is plotted against C_L. The slight defect in lift, acting at the rear of the section makes the predicted aerodynamic centre further forward than the experimental one, as shown. The error—about $0{\cdot}008c$—is noticeable but not serious. The present method would need refinement, however, before being applied to the calculation of hinge moments on flaps, where the wing camber is large near the trailing edge.

It has already been remarked in section 3.2 that, within the incidence range tested, Fig. 10 shows no consistent effect on the lift of fixing transition further forward on both surfaces. Although the position of transition will, in general, affect the asymmetry of the boundary layer on the two surfaces it is possible that in this particular case the larger increase of turbulent flow on the lower surface and the more adverse pressure gradient on the upper surface might cause increases in δ^* which tend to offset each other and leave the lift almost unchanged.

6. *Conclusions.*—From the pressure and boundary-layer measurements it was found that :

(*a*) The lift slope is less than in a perfect non-viscous fluid, even in the limit as $C_L \to 0$. It decreases linearly as C_L increases.

(*b*) The form drag is almost negligible at $C_L = 0$ but increases more rapidly than C_L^2.

(*c*) The aerodynamic centre is slightly ahead of the quarter-chord point and does not change with C_L.

(*d*) At $C_{L\max}$ the suction peak near the leading edge breaks down due to laminar separation without reattachment. On this section no separation was observed near the trailing edge.

(*e*) The pressure distribution in viscous flow and the loss of lift due to the boundary layer may be satisfactorily calculated if the boundary layer is known. The aerodynamic centre is not so well predicted and the calculated form drag is only about half the measured value.

(*f*) Present methods of calculating the turbulent boundary layer are satisfactory for estimating its growth but are handicapped by insufficient initial knowledge of conditions at transition and at the trailing edge.

(*g*) At transition a slight dip in the pressure distribution was observed, which has very little effect on the forces. The position of transition determines the asymmetry in the growth of the boundary layer on the two surfaces which is responsible for the reduction of lift.

Acknowledgment.—The authors are indebted to Mr. D. J. Kettle who helped in the experimental work and to Miss M. Patterson for most of the computing.

NOTATION

x, z	Rectangular co-ordinates, parallel and perpendicular to the chord respectively, on the two-dimensional wing
z'	Distance above aerofoil surface, perpendicular to chord-line
c	Wing chord
t	Wing thickness
p	Static pressure
p_0	Static pressure in free stream
q_0	Dynamic pressure in free stream
V	Velocity
V_0	Velocity in free stream
C_p	Pressure coefficient $= (p - p_0)/q_0$
ΔC_p	Difference of C_p's on upper and lower surfaces
H	Stagnation pressure : *i.e.*, total head
R	Reynolds number
α	Geometric incidence
$\Delta\alpha$	Change of effective incidence due to boundary layer
δ	Boundary-layer thickness
δ^*	Displacement thickness
θ	Momentum thickness
δ^*/θ	Form parameter
C_N	Normal force coefficient
C_T	Tangential force coefficient
C_L	Lift coefficient
C_D	Form-drag coefficient
h	Aerodynamic centre
a_0	Two-dimensional lift slope
$(a_0)_T$	Two-dimensional lift slope in a perfect non-viscous fluid
K_2	Factor to take account of Taylor vorticity condition
U.S.	Suffix indicating upper surface
L.S.	Suffix indicating lower surface

REFERENCES

No.	*Author*	*Title, etc.*
1	J. H. Preston	The calculation of lift taking account of the boundary layer. R. & M. 2725. November, 1949.
2	D. Küchemann, J. Weber and G. G. Brebner.	Low-speed tests on wings of 45-deg sweep. Part II : Balance and pressure measurements on wings of different aspect ratios. R. & M. 2882. May, 1951.
3	W. E. Gray	A simple visual method of recording boundary-layer transition (liquid film). R.A.E. Tech. Note Aero. 1816. A.R.C. 10,028. August, 1946.
4	D. E. Gault	Boundary-layer and stalling characteristics of the NACA 63–009 airfoil section. N.A.C.A. Tech. Note 1894. June, 1949.
5	J. Weber	A simple method for calculating the chordwise pressure distribution on two-dimensional and swept wings for aerofoils of finite thickness. R.A.E. Report Aero. 2391. A.R.C. 13,757. August, 1950.
6	R. C. Pankhurst and H. B. Squire ..	Calculated pressure distributions for the RAE 100–104 aerofoil sections. C.P. 80. March, 1950.
7	E. C. Maskell	Approximate calculation of the turbulent boundary layer in two-dimensional incompressible flow. R.A.E. Report Aero. 2443. A.R.C. 14,654. November, 1951.
8	D. A. Spence	The growth of turbulent boundary layers. A.R.C. 14,162. July, 1951.
9	H. B. Squire and A. D. Young ..	The calculation of the profile drag of aerofoils. R. & M. 1838. November, 1937.
10	H. B. Squire and N. E. Winterbottom	Note on further wing profile drag calculations. R.A.E. Report B.A. 1634. A.R.C. 4871. October, 1940.

TABLE 1

Pressure Coefficients at $R = 1{\cdot}6 \times 10^6$

Upper surface $V_0 = 100$ f.p.s. Free transition

C_p

$\frac{x}{c}$	α (deg)										
	−11·20	−10·48	−9·20	−8·18	−7·16	−6·14	−5·11	−4·09	−3·07	−2·05	−1·02
0	−2·016	−6·585	−4·897	−3·752	−2·630	−1·694	−0·852	−0·167	+0·353	+0·709	+0·944
0·005	+0·747	−0·011	+0·376	+0·624	+0·810	+0·942	+1·006	+0·999	0·919	0·767	0·535
0·008	0·989	+0·366	0·643	0·811	0·924	0·992	1·006	0·952	0·640	0·657	0·408
0·012	0·968	0·770	0·897	0·961	0·987	0·982	0·932	0·839	0·695	0·518	0·276
0·024	0·936	1·004	0·985	0·955	0·901	0·826	0·723	0·601	0·450	0·275	+0·078
0·049	0·756	0·897	0·823	0·759	0·678	0·595	0·480	0·367	0·242	0·099	−0·056
0·074	0·610	0·766	0·680	0·612	0·532	0·449	0·343	0·245	0·128	+0·001	−0·128
0·098	0·520	0·665	0·586	0·517	0·436	0·356	0·256	0·169	+0·064	−0·053	−0·160
0·149	0·380	0·521	0·440	0·376	0·303	0·241	0·154	0·080	−0·010	−0·103	−0·192
0·198	0·279	0·411	0·337	0·277	0·214	0·157	+0·078	0·016	−0·062	−0·146	−0·218
0·298	0·143	0·253	0·194	0·148	0·087	0·049	−0·021	−0·068	−0·129	−0·194	−0·245
0·349	0·093	0·216	0·159	0·114	0·064	0·031	−0·036	−0·074	−0·127	−0·187	−0·232
0·397	0·075	0·194	0·141	0·105	0·056	0·025	−0·034	−0·066	−0·113	−0·166	−0·206
0·448	0·055	0·173	0·125	0·091	0·049	0·023	−0·029	−0·058	−0·096	−0·146	−0·180
0·497	0·045	0·158	0·119	0·089	0·049	0·029	−0·018	−0·046	−0·083	−0·123	−0·159
0·548	0·039	0·153	0·116	0·091	0·056	0·039	−0·002	−0·025	−0·058	−0·095	−0·124
0·597	0·025	0·141	0·109	0·088	0·056	0·043	+0·004	−0·018	−0·048	−0·081	−0·105
0·649	0·017	0·135	0·107	0·088	0·059	0·049	0·014	−0·002	−0·030	−0·062	−0·075
0·696	0·012	0·131	0·107	0·091	0·068	0·060	0·026	+0·014	−0·012	−0·037	−0·032
0·748	+0·010	0·135	0·116	0·103	0·080	0·080	0·046	0·036	+0·014	+0·011	−0·002
0·796	−0·010	0·123	0·109	0·099	0·080	0·082	0·052	0·050	0·040	0·011	+0·004
0·848	−0·028	0·112	0·105	0·099	0·085	0·088	0·058	0·061	0·054	0·033	0·028
0·897	−0·046	0·112	0·111	0·107	0·097	0·104	0·074	0·088	0·074	0·055	0·058
0·948	−0·092	0·099	0·103	0·107	0·103	0·114	0·094	0·105	0·097	0·091	0·091
0·968	−0·124	0·089	0·099	0·105	0·103	0·116	0·104	0·113	0·110	0·107	0·110
1·000	−0·135	+0·064	+0·114	+0·120	+0·119	—	+0·147	+0·146	+0·161	+0·153	+0·158

TABLE 1—*continued*

Upper surface $V_0 = 100$ f.p.s. Free transition

C_p

$\frac{x}{c}$	α (deg)												
	0	1·02	2·05	3·07	4·09	5·11	6·14	7·16	8·18	9·20	10·22	10·73	11·20
0	+0·999	+0·932	+0·710	+0·314	−0·214	−0·926	−1·800	−2·860	−3·946	−5·206	−6·553	−6·961	−1·766
0·005	0·212	−0·173	−0·626	−1·160	−1·739	−2·407	−3·090	−3·840	−4·568	−5·565	−6·742	−6·955	−1·386
0·008	+0·074	−0·303	−0·740	−1·243	−1·777	−2·163	−2·990	−3·618	−4·350	−5·302	−6·381	−5·767	−1·431
0·012	−0·018	−0·337	−0·702	−1·119	−1·549	−1·999	−2·522	−3·280	−4·141	−4·506	−4·731	−4·993	−1·354
0·024	−0·150	−0·388	−0·653	−0·934	−1·237	−1·634	−1·777	−2·149	−2·556	−2·957	−3·372	−3·041	−1·417
0·049	−0·224	−0·395	−0·580	−0·776	−0·972	−1·174	−1·403	−1·636	−1·894	−2·121	−2·372	−2·417	−1·372
0·074	−0·269	−0·414	−0·565	−0·725	−0·897	−1·068	−1·235	−1·411	−1·610	−1·782	−1·983	−2·014	−1·403
0·098	−0·283	−0·408	−0·535	−0·668	−0·806	−0·947	−1·089	−1·235	−1·390	−1·545	−1·673	−1·723	−1·064
0·149	−0·288	−0·387	−0·486	−0·603	−0·687	−0·798	−0·915	−1·012	−1·139	−1·258	−1·341	−1·398	−1·211
0·198	−0·299	−0·380	−0·464	−0·555	−0·630	−0·715	−0·805	−0·902	−0·988	−1·077	−1·145	−1·190	−1·157
0·298	−0·311	−0·368	−0·428	−0·488	−0·559	−0·617	−0·680	−0·737	−0·802	−0·868	−0·906	−0·931	−0·987
0·349	−0·285	−0·341	−0·391	−0·436	−0·496	−0·543	−0·599	−0·646	−0·705	−0·754	−0·782	−0·808	−0·887
0·397	−0·251	−0·303	−0·353	−0·383	−0·436	−0·477	−0·511	−0·562	−0·611	−0·656	−0·680	−0·698	−0·799
0·448	−0·219	−0·266	−0·304	−0·335	−0·378	−0·414	−0·457	−0·486	−0·528	−0·559	−0·583	−0·594	−0·739
0·497	−0·192	−0·236	−0·236	−0·282	−0·319	−0·348	−0·385	−0·416	−0·445	−0·477	−0·491	−0·526	−0·671
0·548	−0·156	−0·160	−0·197	−0·228	−0·264	−0·290	−0·320	−0·341	−0·369	−0·397	−0·408	−0·422	−0·617
0·597	−0·113	−0·142	−0·171	−0·197	−0·225	−0·248	−0·273	−0·290	−0·318	−0·338	−0·338	−0·351	−0·569
0·649	−0·082	−0·115	−0·136	−0·156	−0·181	−0·197	−0·222	−0·255	−0·258	−0·273	−0·276	−0·285	−0·519
0·696	−0·055	−0·079	−0·097	−0·114	−0·135	−0·152	−0·169	−0·180	−0·200	−0·220	−0·219	−0·225	−0·481
0·748	−0·023	−0·044	−0·056	−0·068	−0·086	−0·101	−0·118	−0·123	−0·138	−0·151	−0·147	−0·153	−0·409
0·796	−0·012	−0·028	−0·040	−0·048	−0·060	−0·070	−0·081	−0·086	−0·099	−0·105	−0·105	−0·112	−0·394
0·848	+0·020	+0·004	−0·002	−0·009	−0·021	−0·027	−0·038	−0·040	−0·050	−0·056	−0·054	−0·062	—
0·897	0·053	0·044	+0·038	+0·039	+0·031	+0·022	+0·014	+0·014	+0·010	+0·001	0	−0·010	−0·306
0·948	0·092	0·093	0·086	0·088	0·079	0·071	0·065	0·066	0·059	0·049	+0·046	+0·040	−0·268
0·968	0·112	0·103	0·105	0·109	0·102	0·091	0·082	0·082	0·076	0·064	0·059	0·028	−0·264
1·000	+0·062	+0·145	+0·143	+0·136	+0·129	+0·095	+0·119	+0·088	+0·093	+0·055	+0·026	+0·072	−0·208

TABLE 1—*continued*

Lower Surface $V_0 = 100$ f.p.s. Free transition

C_p

$\frac{x}{c}$	α (deg)										
	−11·20	−10·48	−9·20	−8·18	−7·16	−6·14	−5·11	−4·09	−3·07	−2·05	−1·02
0	−1·906	−7·108	−5·309	−4·078	−2·896	−1·893	−1·001	−0·269	+0·278	+0·670	+0·923
0·007	−1·708	−6·702	−5·309	−4·384	−3·555	−2·935	−2·317	−1·690	−1·131	−0·655	−0·196
0·008	−2·048	−6·710	−5·246	−4·244	−3·434	−2·832	−2·255	−1·680	−1·164	−0·714	−0·274
0·014	−2·181	−4·263	−3·515	−3·819	−3·243	−2·490	−1·906	−1·445	−1·041	−0·681	−0·326
0·027	−1·908	−3·264	−2·785	−2·442	−2·016	−1·656	−1·630	−1·220	−0·928	−0·667	−0·398
0·051	−1·595	−2·249	−2·034	−1·841	−1·632	−1·390	−1·107	−1·006	−0·796	−0·609	−0·409
0·075	−1·680	−1·968	−1·733	−1·556	−1·392	−1·211	−1·042	−0·897	−0·725	−0·578	−0·415
0·101	−1·443	−1·699	−1·505	−1·381	−1·243	−1·090	−0·946	−0·791	−0·683	−0·557	−0·417
0·150	−1·300	−1·383	−1·255	−1·142	−1·036	−0·920	−0·809	−0·689	−0·603	−0·505	−0·394
0·201	−1·166	−1·196	−1·120	−1·009	−0·926	−0·834	−0·745	−0·648	−0·578	−0·497	−0·402
0·299	−0·891	−0·925	−0·870	−0·805	−0·752	−0·689	−0·623	−0·557	−0·491	−0·446	−0·377
0·349	−0·825	−0·801	−0·754	−0·704	−0·657	−0·604	−0·551	−0·490	−0·431	−0·402	−0·340
0·399	−0·735	−0·703	−0·659	−0·615	−0·576	−0·533	−0·489	−0·436	−0·387	−0·370	−0·309
0·449	−0·694	−0·610	−0·580	−0·541	−0·510	−0·474	−0·434	−0·389	−0·348	−0·313	−0·282
0·500	−0·616	−0·508	−0·481	−0·448	−0·420	−0·391	−0·359	−0·317	−0·284	−0·243	−0·234
0·549	−0·577	−0·421	−0·404	−0·375	−0·359	−0·329	−0·302	−0·263	−0·240	−0·205	−0·164
0·600	−0·510	−0·357	−0·342	−0·319	−0·304	−0·281	−0·258	−0·226	−0·205	−0·181	−0·145
0·649	−0·485	−0·291	−0·280	−0·259	−0·248	−0·230	−0·209	−0·181	−0·166	−0·143	−0·115
0·700	−0·422	−0·220	−0·213	−0·197	−0·189	−0·173	−0·156	−0·131	−0·115	−0·097	−0·076
0·749	−0·397	−0·165	−0·165	−0·151	−0·146	−0·132	−0·114	−0·096	−0·087	−0·074	−0·054
0·799	−0·339	−0·108	−0·105	−0·094	−0·090	−0·084	−0·066	−0·053	−0·046	−0·036	−0·023
0·850	−0·324	−0·064	−0·060	−0·053	−0·052	−0·048	−0·033	−0·023	−0·021	−0·014	−0·004
0·899	−0·271	−0·011	−0·005	+0·001	0	0	+0·010	+0·019	+0·020	+0·022	+0·030
0·950	−0·260	+0·035	+0·044	0·053	+0·054	+0·052	0·069	0·073	0·070	0·072	0·074
0·969	−0·230	0·059	0·070	0·083	0·084	0·086	0·097	0·106	0·105	0·107	0·111
1·000	−0·220	+0·081	+0·093	+0·109	+0·114	+0·118	+0·138	+0·144	+0·147	+0·153	+0·153

TABLE 1—*continued*

Lower Surface $V_0 = 100$ f.p.s. Free transition

C_p

$\frac{x}{c}$	α (deg)												
	0	1·02	2·05	3·07	4·09	5·11	6·14	7·16	8·18	9·20	10·22	10·73	11·21
0	+0·999	+0·941	+0·729	+0·353	−0·153	−0·830	−1·405	−2·748	−3·823	−5·056	−6·403	−6·833	−1·463
0·007	0·190	0·481	0·713	0·871	+0·964	+0·992	+0·990	+0·891	+0·748	+0·542	+0·300	+0·161	+0·891
0·008	+0·107	0·403	0·642	0·823	0·933	0·986	1·014	0·949	0·850	0·686	0·494	0·380	0·954
0·014	−0·010	0·248	0·472	0·653	0·792	0·900	0·854	0·909	0·946	0·936	0·860	0·876	0·877
0·027	−0·153	+0·058	0·250	0·424	0·565	0·692	0·805	0·886	0·945	0·977	0·997	1·000	0·908
0·051	−0·225	−0·064	0·093	0·234	0·361	0·478	0·593	0·688	0·762	0·823	0·883	0·902	0·738
0·075	−0·263	−0·128	+0·003	0·125	0·234	0·341	0·450	0·539	0·616	0·687	0·752	0·775	0·581
0·101	−0·287	−0·168	−0·052	+0·056	0·155	0·252	0·351	0·436	0·510	0·575	0·641	0·671	0·499
0·150	−0·289	−0·194	−0·099	−0·008	+0·072	0·155	0·236	0·314	0·382	0·420	0·503	0·528	0·377
0·201	−0·314	−0·234	−0·151	−0·077	−0·004	+0·068	0·143	0·213	0·271	0·330	0·391	0·408	0·284
0·299	−0·312	−0·248	−0·186	−0·129	−0·070	−0·013	0·050	0·103	0·153	0·204	0·249	0·265	0·135
0·349	−0·281	−0·228	−0·173	−0·121	−0·070	−0·018	0·025	0·085	0·128	0·170	0·212	0·230	0·101
0·399	−0·253	−0·207	−0·159	−0·105	−0·070	−0·024	0·023	0·065	0·103	0·143	0·184	0·198	0·074
0·449	−0·234	−0·190	−0·146	−0·107	−0·069	−0·028	0·015	0·054	0·088	0·122	0·158	0·170	0·049
0·500	−0·189	−0·148	−0·109	−0·076	−0·040	−0·002	0·037	0·069	0·099	0·129	0·160	0·173	0·055
0·549	−0·161	−0·122	−0·085	−0·058	−0·026	+0·006	0·043	0·071	0·097	0·123	0·149	0·164	0·045
0·600	−0·113	−0·106	−0·072	−0·045	−0·018	0·012	0·045	0·069	0·091	0·116	0·141	0·148	0·030
0·649	−0·078	−0·068	−0·057	−0·029	−0·006	0·020	0·052	0·073	0·093	0·112	0·135	0·144	0·022
0·700	−0·048	−0·019	−0·013	−0·003	+0·020	0·040	0·069	0·087	0·103	0·120	0·139	0·148	0·022
0·749	−0·028	−0·009	+0·015	+0·009	0·028	0·048	0·075	0·089	0·103	0·118	0·131	0·141	+0·009
0·799	0	+0·015	0·035	0·045	0·040	0·058	0·089	0·095	0·109	0·120	0·129	0·137	−0·001
0·850	+0·014	0·025	0·039	0·046	0·051	0·062	0·089	0·093	0·103	0·108	0·118	0·122	−0·025
0·899	0·040	0·046	0·056	0·056	0·070	0·076	0·097	0·103	0·107	0·108	0·113	0·115	−0·047
0·950	0·084	0·089	0·097	0·090	0·095	0·089	0·107	0·108	0·107	0·102	0·101	0·101	−0·099
0·969	0·117	0·119	0·125	0·121	0·118	0·114	0·123	0·123	0·117	0·110	0·107	0·105	−0·106
1·000	+0·159	+0·159	+0·157	+0·147	+0·141	+0·135	+0·128	+0·125	+0·115	+0·100	+0·086	+0·077	−0·216

TABLE 1—*continued*

Upper surface $V_0 = 100$ f.p.s. Transition fixed at $0{\cdot}15c$ on both surfaces

C_p

$\frac{x}{c}$	α (deg)								
	−4·09	−3·07	−2·05	−1·02	0	+1·02	+2·05	+3·07	+4·09
0	−0·184	+0·330	+0·715	+0·937	+1·001	+0·939	+0·701	+0·292	−0·240
0·005	+1·001	0·925	0·770	0·530	0·211	−0·171	−0·645	−1·188	−1·757
0·008	0·959	0·843	0·658	0·401	+0·072	−0·303	−0·761	−1·272	−1·796
0·012	0·841	0·701	0·516	0·273	−0·019	−0·336	−0·721	−1·143	−1·563
0·024	0·612	0·463	0·292	+0·094	−0·135	−0·378	−0·651	−0·947	−1·239
0·049	0·383	0·255	0·116	−0·046	−0·209	−0·387	−0·580	−0·786	−0·986
0·074	0·252	0·139	+0·013	−0·128	−0·264	−0·415	−0·570	−0·739	−0·884
0·098	0·180	+0·078	−0·034	−0·152	−0·272	−0·401	−0·537	−0·680	−0·788
0·198	+0·037	−0·044	−0·122	−0·199	−0·278	−0·358	−0·446	−0·537	−0·628
0·298	−0·059	−0·124	−0·181	−0·248	−0·305	−0·370	−0·438	−0·506	−0·558
0·349	−0·064	−0·122	−0·169	−0·230	−0·280	−0·336	−0·393	−0·457	−0·498
0·397	−0·057	−0·105	−0·150	−0·199	−0·244	−0·293	−0·346	−0·396	−0·437
0·448	−0·051	−0·093	−0·134	−0·177	−0·217	−0·262	−0·305	−0·351	−0·378
0·497	−0·033	−0·069	−0·108	−0·146	−0·178	−0·214	−0·256	−0·292	−0·320
0·548	−0·019	−0·053	−0·085	−0·122	−0·147	−0·177	−0·212	−0·249	−0·269
0·597	−0·012	−0·044	−0·071	−0·103	−0·127	−0·154	−0·183	−0·212	−0·250
0·649	+0·003	−0·026	−0·051	−0·077	−0·096	−0·126	−0·146	−0·171	−0·183
0·696	0·022	−0·001	−0·028	−0·051	−0·066	−0·087	−0·108	−0·133	−0·138
0·748	0·047	+0·025	+0·006	−0·018	−0·029	−0·049	−0·067	−0·084	−0·091
0·796	0·047	0·031	0·013	−0·006	−0·016	−0·034	−0·047	−0·063	−0·064
0·848	0·061	0·047	0·037	+0·019	+0·016	+0·002	−0·012	−0·024	−0·025
0·897	0·080	0·068	0·061	0·049	0·047	0·037	+0·031	+0·021	+0·022
0·948	0·102	0·092	0·088	0·082	0·082	0·076	0·070	0·065	0·071
0·968	0·110	0·104	0·102	0·096	0·100	0·094	0·092	0·086	0·092
1·000	+0·114	+0·110	+0·139	+0·135	+0·133	+0·127	+0·123	+0·131	+0·119

TABLE 1—*continued*

Lower surface $V_0 = 100$ f.p.s. Transition fixed at $0{\cdot}15c$ on both surfaces

C_p

$\frac{x}{c}$	α (deg)								
	−4·09	−3·07	−2·05	−1·02	0	+1·02	+2·05	+3·07	+4·09
0	−0·305	+0·261	+0·679	+0·926	+0·997	+0·947	+0·727	+0·341	−0·175
0·007	−1·707	−1·155	−0·651	−0·200	0·193	0·480	0·720	0·882	+0·972
0·008	−1·697	−1·188	−0·709	−0·278	+0·109	0·400	0·649	0·830	0·940
0·014	−1·463	−1·061	−0·680	−0·332	−0·007	0·243	0·477	0·663	0·796
0·027	−1·230	−0·938	−0·662	−0·399	−0·151	+0·058	0·262	0·433	0·579
0·051	−1·017	−0·804	−0·605	−0·411	−0·217	−0·059	0·098	0·242	0·375
0·075	−0·892	−0·731	−0·576	−0·416	−0·257	−0·126	+0·008	0·128	0·245
0·101	−0·788	−0·684	−0·553	−0·416	−0·278	−0·164	−0·046	+0·059	0·165
0·201	−0·654	−0·558	−0·467	−0·382	−0·292	−0·216	−0·140	−0·063	+0·012
0·299	−0·560	−0·500	−0·440	−0·370	−0·299	−0·241	−0·180	−0·125	−0·061
0·349	−0·493	−0·442	−0·391	−0·334	−0·273	−0·218	−0·168	−0·121	−0·061
0·399	−0·437	−0·394	−0·355	−0·299	−0·248	−0·203	−0·157	−0·115	−0·063
0·449	−0·391	−0·356	−0·318	−0·272	−0·225	−0·187	−0·147	−0·109	−0·063
0·500	−0·320	−0·289	−0·259	−0·219	−0·175	−0·143	−0·107	−0·075	−0·034
0·549	−0·269	−0·241	−0·216	−0·182	−0·143	−0·118	−0·082	−0·054	−0·017
0·600	−0·230	−0·208	−0·187	−0·157	−0·124	−0·101	−0·069	−0·048	−0·011
0·649	−0·184	−0·167	−0·149	−0·123	−0·093	−0·071	−0·046	−0·025	+0·006
0·700	−0·136	−0·121	−0·104	−0·056	−0·057	−0·040	−0·015	+0·004	0·027
0·749	−0·100	−0·089	−0·076	−0·056	−0·034	−0·023	−0·004	0·011	0·035
0·799	−0·058	−0·048	−0·037	−0·011	−0·003	+0·006	+0·019	0·033	0·054
0·850	−0·027	−0·023	−0·014	−0·002	+0·010	0·017	0·027	0·042	0·056
0·899	+0·015	+0·017	+0·021	+0·029	0·039	0·044	0·048	0·061	0·071
0·950	0·067	0·067	0·069	0·073	0·081	0·081	0·084	0·088	0·096
0·969	0·100	0·100	0·102	0·104	0·107	0·107	0·111	0·111	0·119
1·000	+0·138	+0·140	+0·140	+0·140	+0·142	+0·140	+0·142	+0·138	+0·140

TABLE 2

Pressure Coefficients at $R = 3{\cdot}2 \times 10^6$

Upper surface $\quad V_0 = 200$ f.p.s. $\quad$ Free transition on both surfaces

C_p

$\frac{x}{c}$	α (deg)								
	−2·20	−1·16	−0·12	−0·92	+1·96	+3·00	+4·04	+6·11	+8·19
0	−0·716	+0·940	−1·000	+0·933	+0·699	+0·303	−0·270	−1·851	−4·126
0·005	0·753	0·518	0·192	−0·178	−0·647	−1·192	−1·813	−3·261	—
0·008	0·646	0·387	+0·055	−0·319	−0·769	−1·281	−1·845	−3·177	—
0·012	0·504	0·270	−0·022	−0·342	−0·717	−1·139	−1·601	−2·703	−3·811
0·024	0·165	+0·079	−0·143	−0·385	−0·651	−0·948	−1·278	−1·930	−2·712
0·049	0·103	−0·048	−0·218	−0·389	−0·580	−0·787	−0·983	−1·442	−1·939
0·074	+0·005	−0·121	−0·268	−0·414	−0·568	−0·733	−0·899	−1·262	−1·652
0·098	−0·040	−0·154	−0·288	−0·409	−0·541	−0·676	−0·819	−1·117	−1·435
0·198	−0·128	−0·209	−0·293	−0·376	−0·462	−0·543	−0·633	−0·815	−1·170
0·298	−0·184	−0·245	−0·310	−0·373	−0·429	−0·500	−0·564	−0·692	−1·004
0·349	−0·161	−0·219	−0·275	−0·332	−0·377	−0·440	−0·492	−0·600	−0·710
0·397	−0·155	−0·202	−0·255	−0·304	−0·338	−0·389	−0·439	−0·531	−0·629
0·448	−0·139	−0·182	−0·230	−0·251	−0·301	−0·343	−0·388	−0·468	−0·545
0·497	−0·116	−0·157	−0·172	−0·213	−0·252	−0·288	−0·327	−0·395	−0·464
0·548	−0·093	−0·109	−0·142	−0·176	−0·208	−0·243	−0·273	−0·330	−0·388
0·597	−0·065	−0·092	−0·125	−0·154	−0·182	−0·207	−0·234	−0·281	−0·331
0·649	−0·042	−0·070	−0·094	−0·119	−0·142	−0·166	−0·188	−0·225	−0·267
0·696	−0·014	−0·037	−0·056	−0·078	−0·099	−0·121	−0·140	−0·174	−0·207
0·748	+0·005	−0·013	−0·030	−0·047	−0·065	−0·083	−0·099	−0·123	−0·151
0·796	0·010	−0·004	−0·016	−0·030	−0·044	−0·046	−0·068	−0·085	−0·108
0·848	0·033	+0·023	+0·014	+0·002	−0·006	−0·017	−0·027	−0·038	−0·055
0·897	0·053	0·046	0·041	0·033	+0·027	+0·022	+0·008	+0·010	−0·003
0·948	0·088	0·084	0·082	0·078	0·076	0·073	0·070	0·067	+0·056
0·968	0·106	0·106	0·106	0·103	0·103	0·099	0·096	0·093	0·080
1·000	+0·133	+0·139	+0·113	+0·110	+0·120	+0·120	+0·122	+0·071	+0·165

TABLE 2—*continued*

Lower surface $V_0 = 200$ f.p.s. Free transition on both surfaces

C_p

$\frac{x}{c}$	α (deg)								
	−2·20	−1·16	−0·12	+0·92	+1·96	+3·00	+4·04	+6·11	+8·19
0	+0·681	+0·927	+1·001	+0·946	+0·730	+0·357	−0·026	−1·720	−3·219
0·007	−0·645	−0·199	0·190	0·498	0·718	0·877	+0·969	+0·969	+0·718
0·008	−0·717	−0·268	+0·101	0·401	0·644	0·823	0·939	0·988	0·815
0·014	−0·694	−0·348	−0·024	0·237	0·461	0·643	0·700	0·964	0·989
0·027	−0·671	−0·410	−0·158	+0·053	0·249	0·419	0·568	0·798	0·941
0·051	−0·615	−0·424	−0·234	−0·070	+0·085	0·227	0·359	0·585	0·763
0·075	−0·587	−0·431	−0·276	−0·140	−0·006	0·116	0·234	0·443	0·620
0·101	−0·559	−0·426	−0·292	−0·172	−0·055	+0·052	+0·158	0·352	0·522
0·201	−0·498	−0·411	−0·320	−0·239	−0·157	−0·080	−0·003	0·146	0·280
0·299	−0·439	−0·388	−0·321	−0·256	−0·194	−0·134	−0·092	0·047	0·157
0·349	−0·418	−0·352	−0·289	−0·237	−0·182	−0·130	−0·076	0·021	0·131
0·399	−0·348	−0·317	−0·261	−0·216	−0·166	−0·121	−0·073	0·022	0·111
0·449	−0·310	−0·260	−0·234	−0·189	−0·146	−0·105	−0·063	0·022	0·102
0·500	−0·260	−0·220	−0·172	−0·160	−0·119	−0·083	−0·045	0·030	0·102
0·549	−0·215	−0·181	−0·141	−0·108	−0·101	−0·066	−0·033	0·034	0·100
0·600	−0·188	−0·159	−0·137	−0·098	−0·065	−0·056	−0·023	0·038	0·095
0·649	−0·143	−0·120	−0·091	−0·065	−0·037	−0·020	−0·010	0·047	0·100
0·700	−0·104	−0·085	−0·062	−0·042	−0·019	+0·002	+0·023	0·056	0·101
0·749	−0·078	−0·063	−0·044	−0·028	−0·008	0·011	0·032	0·063	0·106
0·799	−0·046	−0·033	−0·017	−0·006	+0·012	0·025	0·043	0·069	0·106
0·850	−0·018	−0·010	+0·003	+0·013	0·029	0·034	0·045	0·079	0·108
0·899	+0·014	+0·017	0·025	0·032	0·039	0·042	0·050	0·072	0·109
0·950	0·070	0·071	0·076	0·079	0·082	0·082	0·086	0·099	0·110
0·969	0·098	0·098	0·101	0·103	0·106	0·103	0·104	0·110	0·118
1·000	+0·152	+0·153	+0·155	+0·153	+0·153	+0·145	+0·140	+0·134	+0·127

TABLE 2—*continued*

Upper surface $V_0 = 200$ f.p.s. Transition fixed at $0{\cdot}15c$ on both surfaces

C_p

$\frac{x}{c}$	α (deg)						
	−2·20	−1·16	−0·12	0·92	1·96	3·00	4·04
0	+0·711	+0·945	+1·010	+0·949	+0·709	+0·292	−0·286
0·005	0·760	0·524	0·208	−0·178	−0·660	−1·209	−1·839
0·008	0·652	0·395	+0·071	−0·321	−0·778	−1·296	−1·885
0·012	0·513	0·271	−0·010	−0·344	−0·726	−1·169	−1·623
0·024	0·281	+0·079	−0·137	−0·390	−0·658	−0·955	−1·294
0·049	0·104	−0·044	−0·213	−0·395	−0·581	−0·786	−0·992
0·074	+0·009	−0·123	−0·263	−0·418	−0·570	−0·734	−0·904
0·098	−0·038	−0·155	−0·275	−0·413	−0·543	−0·676	−0·819
0·198	−0·118	−0·201	−0·280	−0·368	−0·447	−0·544	−0·638
0·298	−0·184	−0·228	−0·305	−0·374	−0·437	−0·501	−0·570
0·349	−0·163	−0·224	−0·272	−0·334	−0·387	−0·440	−0·498
0·397	−0·151	−0·202	−0·254	−0·300	−0·346	−0·390	−0·441
0·448	−0·137	−0·182	−0·240	−0·267	−0·307	−0·345	−0·389
0·497	−0·110	−0·148	−0·199	−0·224	−0·258	−0·291	−0·329
0·548	−0·088	−0·120	−0·166	−0·186	−0·215	−0·244	−0·274
0·597	−0·072	−0·102	−0·143	−0·160	−0·186	−0·210	−0·237
0·649	−0·046	−0·073	−0·097	−0·123	−0·145	−0·165	−0·187
0·696	−0·019	−0·041	—	—	—	—	−0·142
0·748	+0·003	−0·016	−0·034	−0·052	−0·069	−0·083	−0·097
0·796	0·013	−0·003	−0·002	−0·014	−0·022	−0·057	−0·067
0·848	0·035	+0·022	—	—	+0·013	−0·019	−0·026
0·897	0·057	0·047	+0·038	+0·031	0·024	+0·019	+0·015
0·948	0·088	0·084	0·079	0·072	0·072	0·069	0·070
0·968	0·106	0·103	0·100	0·096	0·095	0·094	0·094
1·000	+0·126	+0·112	+0·124	+0·116	+0·127	+0·104	+0·150

TABLE 2—*continued*

Lower surface $V_0 = 200$ f.p.s. Transition fixed at $0 \cdot 15c$ on both surfaces

C_p

$\frac{x}{c}$	α (deg)						
	−2·20	−1·16	−0·12	+0·92	1·96	3·00	4·04
0	+0·676	+0·933	+0·997	+0·946	+0·724	+0·342	−0·205
0·007	−0·661	−0·279	0·180	0·483	0·720	0·879	+0·976
0·008	−0·732	−0·282	+0·088	0·396	0·645	0·826	0·944
0·014	−0·703	−0·339	−0·036	+0·228	0·464	0·562	0·799
0·027	−0·678	−0·406	−0·165	−0·052	0·252	0·424	0·577
0·051	−0·620	−0·421	−0·238	−0·073	+0·089	0·233	0·368
0·075	−0·588	−0·427	−0·278	−0·139	−0·002	0·124	0·248
0·101	−0·557	−0·420	−0·292	−0·170	−0·050	+0·063	0·169
0·201	−0·485	−0·397	−0·313	−0·232	−0·148	−0·072	+0·010
0·299	−0·447	−0·383	−0·315	−0·255	−0·190	−0·127	−0·063
0·349	−0·397	−0·339	−0·285	−0·231	−0·175	−0·118	−0·065
0·399	−0·352	−0·303	−0·256	−0·209	−0·158	−0·110	−0·062
0·449	−0·311	−0·268	−0·229	−0·188	−0·143	−0·099	−0·056
0·500	−0·263	−0·224	−0·190	−0·154	−0·115	−0·076	−0·038
0·549	−0·217	−0·184	−0·155	−0·123	−0·089	−0·054	−0·021
0·600	−0·188	−0·159	−0·134	−0·107	−0·075	−0·046	−0·016
0·649	−0·145	−0·120	−0·098	−0·075	−0·048	−0·021	+0·004
0·700	−0·105	−0·085	−0·068	−0·047	−0·026	+0·004	0·020
0·749	−0·079	−0·063	−0·048	−0·031	−0·011	0·009	0·029
0·799	−0·046	−0·032	−0·022	−0·007	+0·010	0·026	0·043
0·850	−0·018	−0·006	+0·001	+0·012	0·024	0·037	0·051
0·899	+0·016	+0·021	0·025	0·032	0·041	0·051	0·061
0·950	0·068	0·071	0·071	0·075	0·081	0·085	0·091
0·969	0·095	0·098	0·094	0·097	0·101	0·104	0·110
1·000	+0·145	+0·146	+0·141	+0·141	+0·142	+0·141	+0·141

TABLE 2—*continued*

Upper surface $V_0 = 200$ f.p.s. Transition fixed at $0 \cdot 15c$ on lower surface only

C_p

$\frac{x}{c}$	α (deg)						
	−4·28	−2·20	−1·16	−0·12	+0·92	1·96	4·04
0	−0·210	+0·725	+0·941	+0·998	+0·923	+0·679	−0·299
0·005	+0·995	0·753	0·506	—	−0·198	−0·683	−1·840
0·008	0·960	0·646	0·372	+0·173	−0·341	−0·806	−1·881
0·012	0·837	0·503	0·256	−0·037	−0·360	−0·744	−1·623
0·024	0·486	0·163	+0·073	−0·154	−0·400	−0·675	−1·294
0·049	0·259	0·099	−0·056	−0·223	−0·401	−0·592	−0·989
0·074	0·244	+0·004	−0·127	−0·274	−0·423	−0·579	−0·905
0·098	0·167	−0·043	−0·159	−0·291	−0·423	−0·552	−0·821
0·198	+0·017	−0·135	−0·211	−0·298	−0·384	−0·472	−0·636
0·298	−0·057	−0·186	−0·248	−0·312	−0·380	−0·435	−0·564
0·349	−0·060	−0·169	−0·225	−0·278	−0·340	−0·383	−0·493
0·397	−0·061	−0·156	−0·207	−0·258	−0·307	−0·346	−0·444
0·448	−0·058	−0·138	−0·186	−0·233	−0·257	−0·305	−0·392
0·497	−0·043	−0·114	−0·162	−0·174	−0·218	−0·259	−0·331
0·548	−0·025	−0·094	−0·112	−0·144	−0·179	−0·215	−0·276
0·597	−0·016	−0·063	−0·098	−0·128	−0·159	−0·188	−0·237
0·649	−0·003	−0·041	−0·073	−0·100	−0·124	−0·147	−0·189
0·696	+0·032	−0·014	−0·039	−0·063	−0·084	−0·104	−0·131
0·748	0·047	+0·006	−0·015	−0·034	−0·053	−0·070	−0·099
0·796	0·043	0·011	−0·007	−0·021	−0·035	−0·048	−0·069
0·848	0·056	0·034	+0·019	+0·007	−0·003	−0·012	−0·027
0·897	0·069	0·053	0·043	0·035	+0·027	+0·021	+0·015
0·948	0·092	0·080	0·080	0·078	0·072	0·070	0·067
0·968	0·106	0·105	0·100	0·091	0·096	0·095	0·093
1·000	+0·087	+0·111	+0·110	+0·117	+0·123	+0·128	+0·112

TABLE 2—*continued*

Lower surface $V_0 = 200$ f.p.s. Transition fixed at $0 \cdot 15c$ on lower surface only

C_p

$\frac{x}{c}$	α (deg)						
	−4·28	−2·20	−1·16	−0·12	+0·92	1·96	4·04
0	−0·322	+0·688	+0·929	+0·998	+0·936	+0·710	−0·218
0·007	−1·750	−0·637	−0·180	0·212	0·499	0·730	+0·974
0·008	−1·753	−0·709	−0·269	+0·118	0·411	0·656	0·944
0·014	−1·507	−0·686	−0·330	−0·008	0·247	0·474	0·800
0·027	−1·272	−0·663	−0·390	−0·145	+0·063	0·260	0·578
0·051	−0·973	−0·609	−0·411	−0·222	−0·063	0·096	0·370
0·075	−0·889	−0·579	−0·420	−0·266	−0·131	+0·003	0·244
0·101	−0·816	−0·550	−0·414	−0·280	−0·161	−0·045	+0·170
0·201	−0·665	−0·480	−0·393	−0·304	−0·227	−0·145	−0·063
0·299	−0·570	−0·438	−0·376	−0·307	−0·243	−0·185	−0·064
0·349	−0·503	−0·392	−0·336	−0·278	−0·227	−0·171	−0·066
0·399	−0·442	−0·348	−0·300	−0·249	−0·204	−0·157	−0·062
0·449	−0·391	−0·309	−0·267	−0·222	−0·183	−0·140	−0·058
0·500	−0·329	−0·258	−0·222	−0·184	−0·150	−0·113	−0·040
0·549	−0·276	−0·213	−0·183	−0·149	−0·119	−0·087	−0·023
0·600	−0·236	−0·184	−0·158	−0·129	−0·111	−0·074	−0·018
0·649	−0·186	−0·142	−0·119	−0·093	−0·070	−0·045	+0·004
0·700	−0·137	−0·101	−0·083	−0·063	−0·044	−0·024	0·018
0·749	−0·108	−0·076	−0·061	−0·043	−0·025	−0·009	0·027
0·799	−0·069	−0·043	−0·031	−0·017	−0·003	+0·012	0·040
0·850	−0·032	−0·015	−0·005	+0·006	+0·016	0·026	0·049
0·899	+0·007	+0·026	+0·024	0·030	0·037	0·044	0·060
0·950	0·066	0·072	0·073	0·078	0·082	0·084	0·091
0·969	0·093	0·099	0·100	0·101	0·104	0·106	0·108
1·000	+0·145	+0·150	+0·150	+0·150	+0·149	+0·147	+0·140

TABLE 3

Coefficients of Normal Force, Tangential Force, Lift, Drag and Aerodynamic Centre Position

$V_0 = 100$ f.p.s. $R = 1{\cdot}6 \times 10^6$

(*a*) Free transition on both surfaces

α (deg)	C_N	C_T	C_L	C_D	$\frac{h}{c}$
0	0	+0·0010	0	+0·0001	—
1·02	0·111	−0·0033	0·111	−0·0013	0·249
2·05	0·218	−0·0059	0·218	+0·0019	0·242
3·07	0·324	−0·0156	0·324	0·0018	0·239
4·09	0·429	−0·0270	0·430	0·0036	0·241
5·12	0·528	−0·0423	0·530	0·0050	0·239
6·14	0·630	−0·0618	0·633	0·0060	0·247
7·16	0·734	−0·0836	0·739	0·0086	0·244
8·18	0·835	−0·1077	0·842	0·0122	0·243
9·20	0·918	−0·1316	0·927	0·0170	0·243
10·22	1·012	−0·1660	1·025	0·0162	0·237
10·48	1·032	−0·1741	1·047	0·0164	0·242
10·73	1·055	−0·1744	1·068	0·0252	0·240
11·20	0·894	−0·0332	0·884	+0·1415	0·310

(*b*) Transition fixed at 0·15*c* on both surfaces

α (deg)	C_N	C_T	C_L	C_D	$\frac{h}{c}$
0	0	+0·0020	0	+0·0020	—
1·02	0·111	−0·0022	0·111	−0·0001	0·243
2·05	0·222	−0·0050	0·222	+0·0030	0·248
3·07	0·333	−0·0138	0·333	0·0041	0·246
4·09	0·434	−0·0283	0·435	+0·0028	0·246

TABLE 4

Coefficients of Normal Force, Tangential Force, Lift, Drag and Aerodynamic Centre Position

$V_0 = 200$ f.p.s. $R = 3{\cdot}2 \times 10^6$

(*a*) Free transition on both surfaces

α (deg)	C_N	C_T	C_L	C_D	$\frac{h}{c}$
−2·20	−0·232	−0·0057	−0·232	0·0032	0·247
−1·16	−0·124	−0·0018	−0·124	0·0008	0·245
−0·12	−0·009	+0·0007	−0·009	0·0007	—
+0·92	+0·099	−0·0016	+0·099	0	0·241
1·96	0·210	−0·0065	0·210	0·0007	0·247
3·00	0·315	−0·0151	0·315	0·0015	0·243
4·04	0·425	−0·0290	0·426	0·0010	0·245
6·11	0·638	−0·0650	0·641	0·0034	0·244
+8·19	+0·859	−0·1157	+0·867	0·0077	0·244

(*b*) Transition fixed at $0{\cdot}15c$ on lower surface only

α (deg)	C_N	C_T	C_L	C_D	$\frac{h}{c}$
−4·28	−0·441	−0·0315	−0·437	0·0016	0·248
−2·20	−0·225	−0·0069	−0·225	0·0017	0·245
−1·16	−0·116	−0·0004	−0·116	0·0020	0·235
−0·12	0	+0·0017	0	0·0017	—
+0·92	+0·109	−0·0014	+0·109	0·0003	0·244
1·96	0·222	−0·0060	0·222	0·0016	0·249
+4·04	+0·436	−0·0272	+0·437	0·0036	0·246

(*c*) Transition fixed at $0{\cdot}15c$ on both surfaces

α (deg)	C_N	C_T	C_L	C_D	$\frac{h}{c}$
−2·20	−0·232	−0·0054	−0·232	0·0036	0·244
−1·16	−0·123	−0·0020	−0·123	0·0005	0·238
−0·12	−0·010	+0·0021	−0·010	0·0021	—
+0·92	+0·098	−0·0014	+0·098	0·0002	0·245
1·96	0·206	−0·0051	0·206	0·0020	0·243
3·00	0·317	−0·0139	0·317	0·0027	0·249
+4·04	+0·427	−0·0277	+0·428	0·0025	0·245

TABLE 5

Coefficients of Normal Force, Tangential Force, Lift, Drag and Aerodynamic Centre Position calculated from the Profile Shape and Boundary-layer Measurements

$V_0 = 100$ f.p.s. $R = 1{\cdot}6 \times 10^6$

α (deg)	C_N	C_T	C_L	C_D	$\frac{h}{c}$
4·09	0·432	−0·0305	0·433	0·0003	0·236
8·18	0·836	−0·1155	0·844	0·0046	0·236

TABLE 6

Position of Free Transition Point

$V_0 = 100$ f.p.s. $R = 1{\cdot}6 \times 10^6$

C_L	Upper surface	Lower surface
0	$\frac{x}{c} = 0{\cdot}62$	$\frac{x}{c} = 0{\cdot}62$
0·111	0·54	0·67
0·218	0·44	0·72
0·324	0·32	0·76
0·430	0·11	0·85
0·530	0·020	0·90
0·633	0·017	
0·739	0·013	
0·842	0·011	
0·927	0·008	

$V_0 = 200$ f.p.s. $R = 3{\cdot}2 \times 10^6$

C_L	Upper surface	Lower surface
−0·232	$\frac{x}{c} = 0{\cdot}58$	$\frac{x}{c} = 0{\cdot}35$
−0·124	0·55	0·43
−0·009	0·50	0·50
+0·099	0·43	0·57
0·210	0·35	0·60
0·315	0·11	
0·426	0·05	
0·641	0·02	
+0·867	0·01	

TABLE 7

Velocity and Total-Head Measurements in the Boundary Layer

$R = 1{\cdot}6 \times 10^6$

$x/c = 1{\cdot}0015$ (trailing edge) : traverse perpendicular to chord-line

$\alpha = 0$ deg			$\alpha = 4{\cdot}09$ deg			$\alpha = 8{\cdot}18$ deg		
$\frac{z'}{c}$	$\frac{V}{V_0}$	$\frac{H-p_0}{q_0}$	$\frac{z'}{c}$	$\frac{V}{V_0}$	$\frac{(H-p_0)}{q_0}$	$\frac{z'}{c}$	$\frac{V}{V_0}$	$\frac{(H-p_0)}{q_0}$
+0·02845	0·953	1·004	+0·03555	0·956	0·997	+0·04979	0·975	0·998
0·02134	0·950	1·008	0·03128	0·951	0·994	0·04694	0·974	0·998
0·01992	0·948	1·006	0·02987	0·950	0·994	0·04552	0·973	0·997
0·01849	0·945	1·002	0·02845	0·946	0·987	0·04409	0·970	0·993
0·01707	0·940	0·997	0·02703	0·938	0·975	0·04267	0·967	0·987
0·01565	0·936	0·992	0·02561	0·927	0·958	0·04125	0·962	0·980
0·01422	0·922	0·969	0·01992	0·836	0·807	0·03982	0·955	0·968
0·00712	0·772	0·738	0·01281	0·679	0·583	0·03555	0·908	0·884
0·00285	0·618	0·548	0·00569	0·501	0·390	0·02845	0·792	0·694
+0·00142	0·540	0·469	0·00285	0·412	0·320	0·02134	0·657	0·505
0	0·368	0·317	0·00142	0·354	0·285	0·01422	0·519	0·352
−0·00142	0·540	0·468	0·00072	0·307	0·259	0·00569	0·354	0·224
−0·00285	0·620	0·553	+0·00036	0·289	0·250	0·00285	0·295	0·192
−0·00427	0·684	0·624	0	0·401	0·335	0·00142	0·257	0·171
−0·00569	0·735	0·687	−0·00017	0·509	0·426	+0·00072	0·226	0·159
−0·00712	0·781	0·748	−0·00036	0·556	0·476	0	0·156	0·132
−0·01422	0·919	0·962	−0·00072	0·609	0·534	−0·00017	0·150	0·131
−0·01565	0·935	0·984	−0·00142	0·656	0·591	−0·00036	0·156	0·132
−0·01707	0·939	0·992	−0·00285	0·748	0·705	−0·00072	0·265	0·178
−0·01849	0·942	0·997	−0·00569	0·878	0·893	−0·00142	0·552	0·410
−0·01992	0·943	0·992	−0·00854	0·929	0·979	−0·00285	0·883	0·880
−0·02134	0·941	0·986	−0·00996	0·937	0·990	−0·00427	0·949	0·984
−0·02845	0·945	0·982	−0·01068	0·940	0·993	−0·00499	0·954	0·996
			−0·01139	0·941	0·993	−0·00569	0·956	0·997
			−0·01422	0·943	0·992	−0·00712	0·955	0·994

TABLE 7—*continued*

$x/c = 0{\cdot}951$: traverse perpendicular to chord-line

$\alpha = 0$ deg			$\alpha = 4{\cdot}09$ deg			$\alpha = 8{\cdot}18$ deg		
$\frac{z'}{c}$	$\frac{V}{V_0}$	$\frac{(H-p_0)}{q_0}$	$\frac{z'}{c}$	$\frac{V}{V_0}$	$\frac{(H-p_0)}{q_0}$	$\frac{z'}{c}$	$\frac{V}{V_0}$	$\frac{(H-p_0)}{q_0}$
			Upper surface			*Upper surface*		
0·0203	0·977	0·994	0·0288	0·959	0·993	0·0472	0·937	0·991
0·0174	0·976	0·994	0·0259	0·959	0·992	0·0401	0·938	0·994
0·0145	0·971	0·985	0·0230	0·954	0·984	0·0358	0·937	0·990
0·0131	0·965	0·973	0·0203	0·938	0·953	0·0330	0·930	0·977
0·0117	0·951	0·947	0·0174	0·900	0·883	0·0302	0·911	0·941
0·0102	0·931	0·909	0·0131	0·805	0·721	0·0259	0·846	0·829
0·0088	0·904	0·860	0·0102	0·741	0·622	0·0188	0·706	0·610
0·0075	0·869	0·800	0·0060	0·621	0·459	0·0117	0·534	0·399
0·0060	0·832	0·736	0·0032	0·538	0·363	0·0046	0·363	0·245
0·0046	0·786	0·663	0·0017	0·481	0·305	0·0017	0·265	0·183
0·0032	0·732	0·583	0·0010	0·437	0·264	0·0010	0·185	0·147
0·0017	0·662	0·484	0·0007	0·407	0·239	0·0007	0·099	0·122
0·0010	0·625	0·437	0·0003	0·345	0·192	0·0003	—	0·113
0·0007	0·579	0·382						
0·0003	0·509	0·306	*Lower surface*			*Lower surface*		
			0·0003	0·480	0·327	0·0003	0·260	0·150
			0·0007	0·555	0·406	0·0007	0·364	0·219
			0·0010	0·604	0·461	0·0010	0·522	0·359
			0·0017	0·695	0·580	0·0014	0·646	0·504
			0·0032	0·852	0·823	0·0017	0·723	0·611
			0·0046	0·924	0·949	0·0025	0·886	0·872
			0·0060	0·943	0·988	0·0032	0·927	0·947
			0·0075	0·948	0·996	0·0046	0·947	0·984
			0·0117	0·949	0·998	0·0060	0·948	0·986
			0·0336	0·949	0·998	0·0075	0·948	0·987

TABLE 7—*continued*

$x/c = 0{\cdot}899$: traverse perpendicular to chord-line

$\alpha = 0$ deg			$\alpha = 4{\cdot}09$ deg			$\alpha = 8{\cdot}18$ deg		
$\frac{z'}{c}$	$\frac{V}{V_0}$	$\frac{(H-p_0)}{q_0}$	$\frac{z'}{c}$	$\frac{V}{V_0}$	$\frac{(H-p_0)}{q_0}$	$\frac{z'}{c}$	$\frac{V}{V_0}$	$\frac{(H-p_0)}{q_0}$
			Upper surface			*Upper surface*		
0·0160	0·982	1·004	0·0259	0·986	0·995	0·0344	0·991	0·989
0·0145	0·982	1·004	0·0245	0·989	0·998	0·0330	0·991	0·989
0·0131	0·979	0·999	0·0230	0·988	0·995	0·0316	0·989	0·985
0·0117	0·968	0·978	0·0216	0·987	0·993	0·0302	0·986	0·977
0·0102	0·958	0·959	0·0203	0·983	0·986	0·0288	0·977	0·962
0·0075	0·902	0·852	0·0188	0·972	0·964	0·0259	0·949	0·906
0·0032	0·758	0·615	0·0174	0·955	0·933	0·0117	0·662	0·444
0·0017	0·685	0·509	0·0102	0·797	0·654	0·0046	0·481	0·237
0·0010	0·641	0·451	0·0032	0·588	0·366	0·0017	0·401	0·166
0·0003	0·518	0·308	0·0017	0·531	0·301	0·0010	0·368	0·141
			0·0010	0·484	0·254	0·0003	0·287	0·078
			0·0003	0·388	0·170	—	—	—
			Lower surface			*Lower surface*		
			0·0003	0·171	0·187	0·0003	0·215	0·154
			0·0010	0·400	0·231	0·0010	0·515	0·372
			0·0017	0·594	0·423	0·0017	0·730	0·640
			0·0025	0·823	0·746	0·0025	0·870	0·864
			0·0032	0·904	0·888	0·0032	0·925	0·963
			0·0039	0·949	0·973	0·0035	0·937	0·984
			0·0042	0·959	0·991	0·0039	0·940	0·991
			0·0046	0·959	0·990	0·0046	0·941	0·993
			0·0060	0·960	0·992	0·0060	0·941	0·994
			0·0075	0·960	0·992	0·0075	0·941	0·994

TABLE 7—*continued*

$x/c = 0{\cdot}795$: traverse perpendicular to chord-line

$\alpha = 0$ deg			$\alpha = 4{\cdot}09$ deg			$\alpha = 8{\cdot}18$ deg		
$\frac{z'}{c}$	$\frac{V}{V_0}$	$\frac{(H-p_0)}{q_0}$	$\frac{z'}{c}$	$\frac{V}{V_0}$	$\frac{(H-p_0)}{q_0}$	$\frac{z'}{c}$	$\frac{V}{V_0}$	$\frac{(H-p_0)}{q_0}$
			Upper surface			*Upper surface*		
0·0145	1·000	0·993	0·0216	1·030	1·001	0·0302	1·084	0·999
0·0117	0·999	0·992	0·0188	1·030	1·001	0·0273	1·084	0·999
0·0102	0·994	0·982	0·0174	1·028	0·996	0·0259	1·039	0·982
0·0075	0·963	0·923	0·0160	1·014	0·966	0·0245	1·032	0·966
0·0060	0·928	0·854	0·0145	0·997	0·934	0·0230	1·020	0·942
0·0046	0·880	0·768	0·0117	0·933	0·810	0·0216	1·001	0·903
0·0032	0·822	0·669	0·0046	0·709	0·442	0·0174	0·912	0·735
0·0017	0·746	0·552	0·0032	0·656	0·371	0·0102	0·724	0·326
0·0003	0·610	0·365	0·0017	0·595	0·294	0·0060	0·606	0·269
			0·0010	0·561	0·255	0·0032	0·520	0·173
			0·0007	0·535	0·226	0·0017	0·470	0·124
			0·0005	0·514	0·204	0·0010	0·439	0·093
			0·0004	0·500	0·190	0·0007	0·402	0·063
			0·0003	0·456	0·148	0·0003	0·335	0·014
			Lower surface			*Lower surface*		
			0·0003	0·230	0·089	0·0003	0·213	0·204
			0·0006	0·411	0·205	0·0006	0·461	0·318
			0·0010	0·512	0·298	0·0010	0·595	0·460
			0·0017	0·763	0·618	0·0013	0·731	0·639
			0·0025	0·911	0·866	0·0017	0·817	0·773
			0·0032	0·964	0·966	0·0025	0·910	0·933
			0·0039	0·979	0·996	0·0032	0·934	0·978
			0·0046	0·981	0·998	0·0039	0·938	0·984
			0·0053	0·983	1·001	0·0046	0·939	0·986
			0·0060	0·982	1·000	0·0053	0·940	0·988
						0·0060	0·939	0·986

TABLE 7—*continued*

$x/c = 0{\cdot}628$: traverse perpendicular to chord-line

$\alpha = 0$ deg			$\alpha = 4{\cdot}09$ deg			$\alpha = 8{\cdot}18$ deg		
$\frac{z'}{c}$	$\frac{V}{V_0}$	$\frac{(H-p_0)}{q_0}$	$\frac{z'}{c}$	$\frac{V}{V_0}$	$\frac{(H-p_0)}{q_0}$	$\frac{z'}{c}$	$\frac{V}{V_0}$	$\frac{(H-p_0)}{q_0}$
			Upper surface			*Upper surface*		
0·0075	1·044	0·993	0·0160	1·086	0·987	0·0230	1·126	−0·992
0·0060	1·045	0·994	0·0145	1·086	0·986	0·0216	1·123	0·987
0·0053	1·044	0·993	0·0138	1·084	0·983	0·0203	1·122	0·984
0·0046	1·043	0·989	0·0131	1·082	0·977	0·0188	1·116	0·970
0·0039	1·041	0·986	0·0117	1·068	0·948	0·0174	1·099	0·934
0·0032	1·015	0·929	0·0102	1·036	0·877	0·0160	1·071	0·872
0·0025	0·951	0·807	0·0032	0·746	0·364	0·0088	0·843	0·440
0·0020	0·874	0·666	0·0025	0·716	0·318	0·0075	0·793	0·354
0·0017	0·756	0·474	0·0017	0·665	0·249	0·0046	0·690	0·202
0·0010	0·565	0·221	0·0010	0·621	0·191	0·0032	0·633	0·125
0·0003	0·395	0·057	0·0007	0·575	0·136	0·0017	0·568	+0·048
			0·0003	0·495	0·051	0·0010	0·517	−0·008
						0·0007	0·482	−0·042
						0·0003	0·410	−0·107
			Lower surface			*Lower surface*		
			0·0003	0·224	0·042	0·0003	0·258	−0·164
			0·0010	0·530	0·272	0·0010	0·608	0·466
			0·0017	0·790	0·616	0·0017	0·817	0·763
			0·0020	0·910	0·819	0·0025	0·928	0·956
			0·0025	0·957	0·908	0·0032	0·943	0·986
			0·0032	0·990	0·972	0·0039	0·946	0·992
			0·0035	0·999	0·989	0·0046	0·946	0·992
			0·0039	1·000	0·992	0·0060	0·946	+0·992
			0·0046	1·000	0·992			
			0·0053	1·000	0·993			
			0·0060	1·000	0·993			
			0·0075	1·000	0·993			

TABLE 7—*continued*

$x/c = 0 \cdot 400$: traverse perpendicular to chord-line

$\alpha = 0$ deg			$\alpha = 4 \cdot 09$ deg			$\alpha = 8 \cdot 18$ deg		
$\frac{z'}{c}$	$\frac{V}{V_0}$	$\frac{(H - p_0)}{q_0}$	$\frac{z'}{c}$	$\frac{V}{V_0}$	$\frac{(H - p_0)}{q_0}$	$\frac{z'}{c}$	$\frac{V}{V_0}$	$\frac{(H - p_0)}{q_0}$
			Upper surface			*Upper surface*		
0·0048	1·119	0·997	0·0119	1·195	0·994	0·0147	1·295	−0·993
0·0041	1·117	0·994	0·0104	1·195	0·994	0·0133	1·263	0·987
0·0034	1·117	0·994	0·0090	1·194	0·992	0·0119	1·252	0·959
0·0027	1·112	0·983	0·0083	1·192	0·989	0·0104	1·226	0·891
0·0019	1·060	0·871	0·0077	1·186	0·974	0·0090	1·169	0·756
0·0016	0·980	0·707	0·0070	1·177	0·953	0·0062	1·038	0·467
0·0012	0·909	0·573	0·0062	1·154	0·900	0·0034	0·872	0·161
0·0010	0·811	0·404	0·0034	1·003	0·573	0·0027	0·827	0·073
0·0009	0·737	0·289	0·0019	0·897	0·372	0·0019	0·784	+0·006
0·0005	0·535	0·033	0·0010	0·807	0·218	0·0013	0·746	−0·053
			0·0005	0·761	0·147	0·0009	0·706	−0·112
						0·0005	0·683	−0·143
			Lower surface			*Lower surface*		
			0·0005	0·575	0·261	0·0005	0·587	−0·449
			0·0007	0·695	0·414	0·0009	0·704	0·604
			0·0009	0·774	0·530	0·0012	0·838	0·806
			0·0012	0·866	0·681	0·0016	0·904	0·921
			0·0016	0·955	0·843	0·0019	0·933	0·973
			0·0019	1·007	0·945	0·0027	0·943	0·994
			0·0022	1·028	0·987	0·0034	0·942	+0·991
			0·0027	1·031	0·993			
			0·0034	1·032	0·994			

TABLE 7—*continued*

$x/c = 0{\cdot}300$: traverse perpendicular to chord-line

$\alpha = 0$ deg			$\alpha = 2{\cdot}05$ deg			$\alpha = 4{\cdot}09$ deg		
$\frac{z'}{c}$	$\frac{V}{V_0}$	$\frac{(H-p_0)}{q_0}$	$\frac{z'}{c}$	$\frac{V}{V_0}$	$\frac{(H-p_0)}{q_0}$	$\frac{z'}{c}$	$\frac{V}{V_0}$	$\frac{(H-p_0)}{q_0}$
			Upper surface			*Upper surface*		
0·0032	1·140	+0·990	0·0046	1·167	+0·991	0·0082	1·243	0·992
0·0025	1·140	0·989	0·0032	1·167	0·991	0·0075	1·244	0·993
0·0020	1·137	0·982	0·0020	1·162	0·979	0·0068	1·243	0·991
0·0017	1·123	0·950	0·0017	1·144	0·939	0·0060	1·240	0·981
0·0014	1·077	0·851	0·0014	1·095	0·827	0·0053	1·232	0·962
0·0010	0·973	0·637	0·0010	0·982	0·495	0·0046	1·211	0·912
0·0008	0·911	0·519	0·0007	0·788	+0·249	0·0032	1·138	0·738
0·0007	0·789	0·313	0·0003	0·498	−0·124	0·0025	1·087	0·627
0·0005	0·673	+0·144				0·0017	1·023	0·492
0·0003	0·525	−0·035				0·0014	0·986	0·417
						0·0010	0·945	0·339
						0·0007	0·896	0·248
						0·0005	0·871	0·204
						0·0003	0·817	0·113
			Lower surface			*Lower surface*		
			0·0003	0·637	+0·221	0·0003	0·534	0·216
			0·0007	0·861	0·557	0·0007	0·772	0·528
			0·0010	0·995	0·804	0·0008	0·873	0·693
			0·0014	1·058	0·935	0·0010	0·926	0·789
			0·0017	1·079	0·981	0·0014	1·006	0·943
			0·0025	1·083	0·990	0·0017	1·022	0·976
			0·0032	1·083	+0·991	0·0020	1·029	0·990
						0·0025	1·029	0·990

TABLE 7—*continued*

$x/c = 0{\cdot}300$—*continued* : traverse perpendicular to chord-line

$\alpha = 6{\cdot}14$ deg			$\alpha = 8{\cdot}18$ deg		
$\frac{z'}{c}$	$\frac{V}{V_0}$	$\frac{(H - p_0)}{q_0}$	$\frac{z'}{c}$	$\frac{V}{V_0}$	$\frac{(H - p_0)}{q_0}$
Upper surface			*Upper surface*		
0·0102	1·286	+0·990	0·0131	1·334	+0·989
0·0088	1·285	0·988	0·0117	1·334	0·990
0·0075	1·274	0·959	0·0102	1·332	0·984
0·0060	1·227	0·841	0·0095	1·327	0·971
0·0046	1·145	0·638	0·0088	1·315	0·941
0·0017	0·937	0·213	0·0075	1·265	0·811
0·0010	0·871	0·096	0·0060	1·188	0·622
0·0007	0·833	+0·030	0·0032	1·001	0·213
0·0003	0·783	−0·051	0·0017	0·892	+0·007
			0·0014	0·852	−0·062
			0·0010	0·829	−0·101
			0·0007	0·795	−0·157
			0·0003	0·738	−0·244
Lower surface			*Lower surface*		
0·0003	0·650	+0·472	0·0003	0·558	+0·473
0·0007	0·833	0·743	0·0004	0·660	0·598
0·0009	0·898	0·854	0·0006	0·727	0·689
0·0011	0·944	0·939	0·0007	0·787	0·781
0·0014	0·961	0·972	0·0010	0·862	0·905
0·0017	0·966	0·983	0·0011	0·882	0·940
0·0025	0·969	0·989	0·0013	0·895	0·962
0·0032	0·970	+0·990	0·0014	0·903	0·977
			0·0017	0·910	0·990
			0·0025	0·914	0·996
			0·0032	0·914	+0·996

TABLE 8

Static Pressure Measurements in the Boundary Layer

$R = 1{\cdot}6 \times 10^6$

$x/c = 1{\cdot}0015$ (trailing edge) : traverse perpendicular to chord-line

$\alpha = 0$ deg		$\alpha = 4{\cdot}09$ deg		$\alpha = 8{\cdot}18$ deg	
$\frac{z'}{c}$	$\frac{(p - p_0)}{q_0}$	$\frac{z'}{c}$	$\frac{(p - p_0)}{q_0}$	$\frac{z'}{c}$	$\frac{(p - p_0)}{q_0}$
+0·02945	0·094	+0·03513	0·083	+0·04367	0·052
0·02234	0·103	0·03228	0·087	0·03655	0·058
0·01522	0·118	0·02519	0·098	0·02945	0·064
0·00812	0·138	0·01807	0·111	0·02234	0·071
0·00669	0·143	0·01096	0·125	0·01522	0·080
0·00527	0·151	0·00669	0·135	0·00812	0·093
0·00385	0·159	0·00385	0·146	0·00669	0·096
0·00242	0·170	0·00242	0·153	0·00527	0·097
+0·001	0·179	+0·001	0·162	0·00385	0·102
−0·001	0·177	−0·001	0·160	0·00242	0·106
−0·00242	0·170	−0·00242	0·150	0·00172	0·105
−0·00385	0·159	−0·00385	0·137	+0·001	0·106
−0·00527	0·148	−0·00527	0·125	−0·001	0·106
−0·00669	0·141	−0·00669	0·120	−0·00242	0·103
−0·00812	0·136	−0·00812	0·115	−0·00385	0·092
−0·01522	0·114	−0·00954	0·111	−0·00527	0·083
−0·02234	0·098	−0·01096	0·108	−0·00669	0·081
−0·02945	0·087	−0·01239	0·106	−0·00812	0·080
		−0·01381	0·103	−0·01096	0·078

TABLE 9

Displacement Thickness, Momentum Thickness and Form Parameter, from Boundary-layer Measurements

$R = 1{\cdot}6 \times 10^6$

α (deg)		$\frac{x}{c}$ 0·300	0·400	0·628	0·795	0·899	0·951	1·000
0	δ^*/c	0·00049	0·00071	0·00103	0·00150	0·00189	0·00218	0·00266
	θ/c	0·00027	0·00035	0·00055	0·00105	0·00138	0·00163	0·00218
	δ^*/θ	1·82	2·03	1·87	1·43	1·37	1·34	1·22
				Upper surface				
2·05	δ^*/c	0·00059						
	θ/c	0·00029						
	δ^*/θ	2·04						
4·09	δ^*/c	0·00078	0·00124	0·00266	0·00355	0·00456	0·00525	0·00731
	θ/c	0·00059	0·00092	0·00168	0·00237	0·00297	0·00335	0·00459
	δ^*/θ	1·32	1·35	1·58	1·50	1·54	1·57	1·59
6·14	δ^*/c	0·00124						
	θ/c	0·00096						
	δ^*/θ	1·29						
8·18	δ^*/c	0·00185	0·00257	0·00480	0·00669	0·00850	0·01105	0·01396
	θ/c	0·00130	0·00176	0·00297	0·00403	0·00493	0·00558	0·00725
	δ^*/θ	1·42	1·46	1·62	1·66	1·73	1·98	1·93
				Lower surface				
2·05	δ^*/c	0·00042						
	θ/c	0·00022						
	δ^*/θ	1·91						
4·09	δ^*/c	0·00045	0·00056	0·00103	0·00106	0·00144	0·00111	0·00155
	θ/c	0·00020	0·00031	0·00046	0·00049	0·00057	0·00071	0·00115
	δ^*/θ	2·25	1·81	2·24	2·16	2·53	1·57	1·35
6·14	δ^*/c	0·00040						
	θ/c	0·00019						
	δ^*/θ	2·10						
8·18	δ^*/c	0·00035	0·00052	0·00088	0·00086	0·00108	0·00108	0·00122
	θ/c	0·00019	0·00026	0·00041	0·00043	0·00051	0·00048	0·00056
	δ^*/θ	1·84	2·00	2·15	2·00	2·12	2·25	2·18

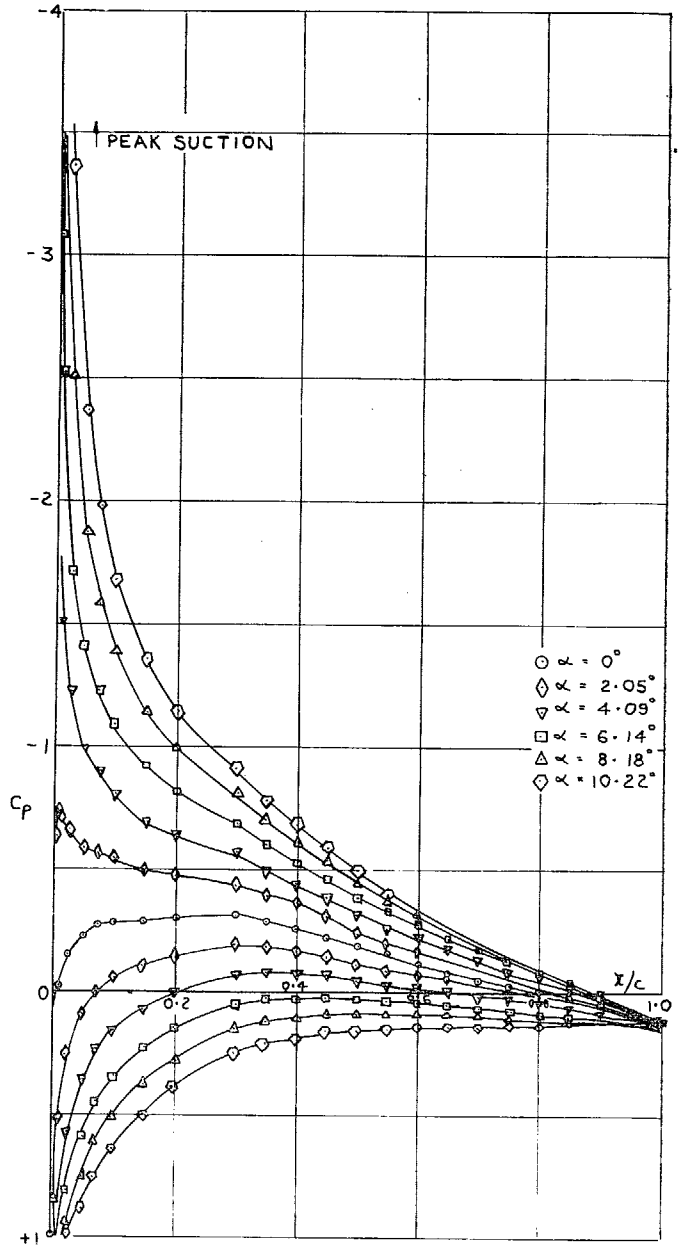

FIG. 1. Chordwise pressure distributions up to the stall.
$R = 1{\cdot}6 \times 10^6$.

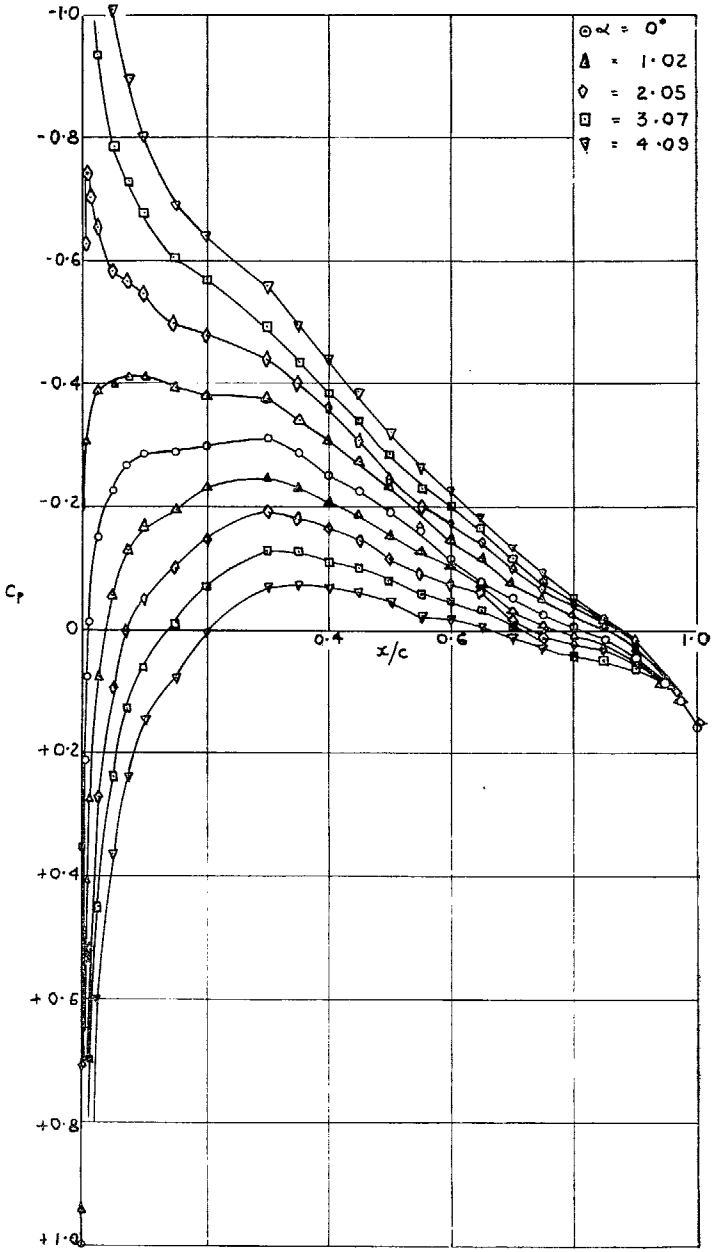

FIG. 2. Chordwise pressure distributions at small incidences.
$R = 1{\cdot}6 \times 10^6$.

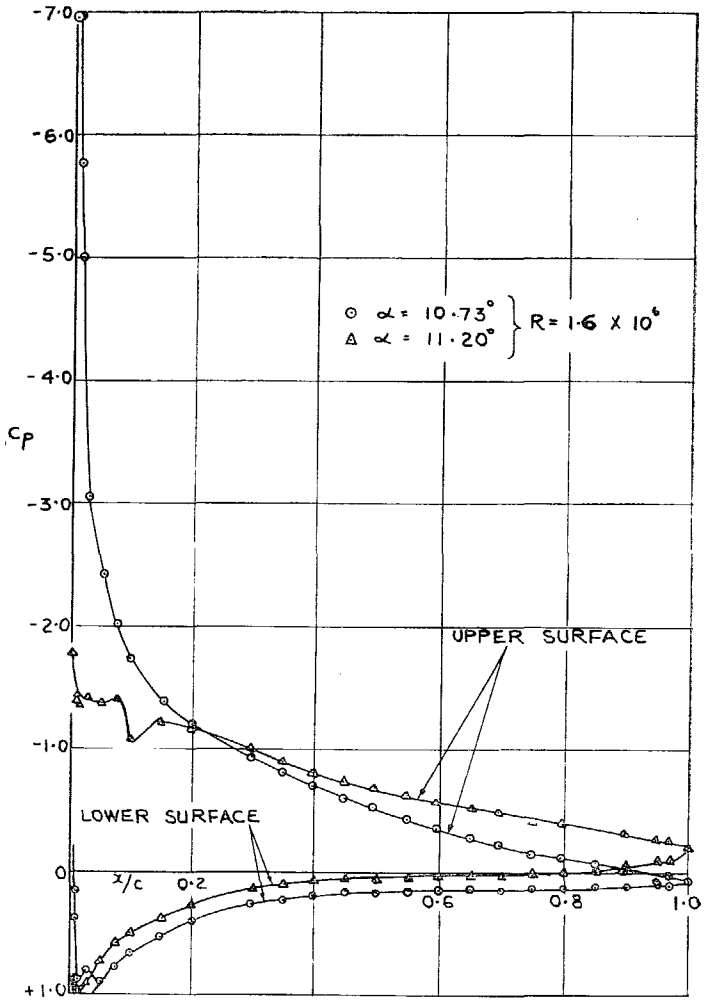

FIG. 3. Pressure distributions near $C_{L\,max}$.

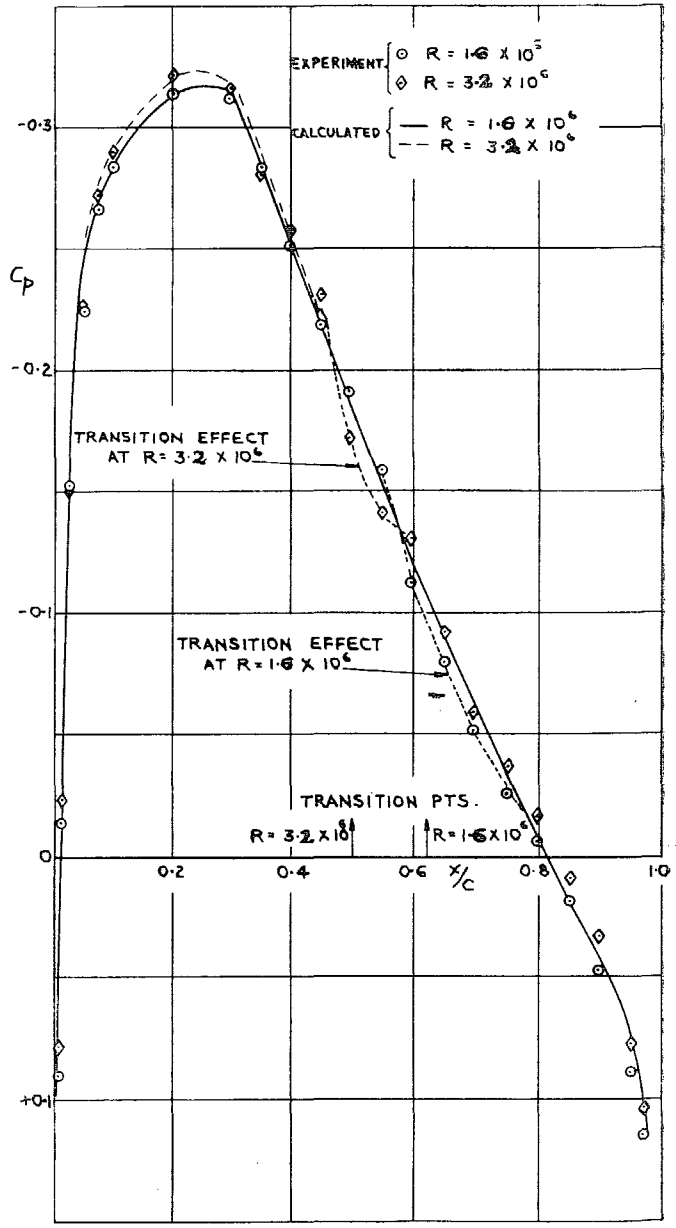

FIG. 4. Pressure distributions at zero incidence. Free transition.

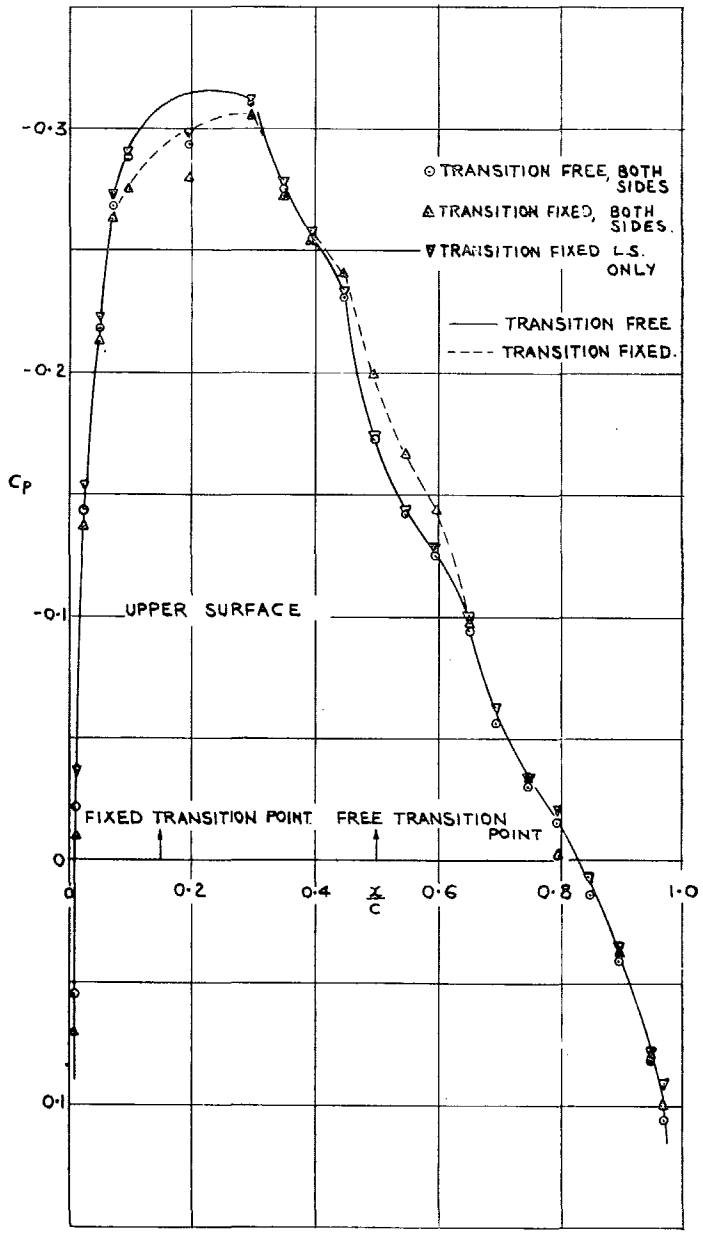

FIG. 5. Effect of fixing transition on the pressure distribution : upper surface. $\alpha = -0{\cdot}12$ deg. $R = 3{\cdot}2 \times 10^6$.

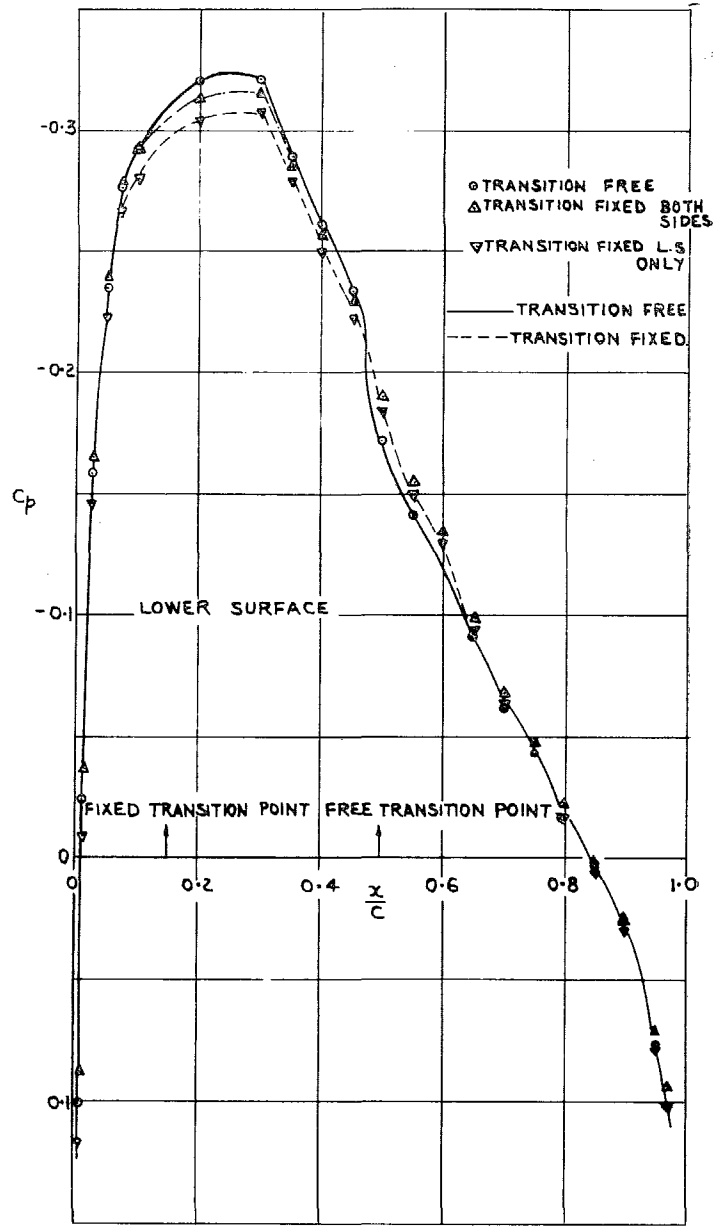

FIG. 6. Effect of fixing transition on the pressure distribution : lower surface. $\alpha = -0{\cdot}12$ deg. $R = 3{\cdot}2 \times 10^6$.

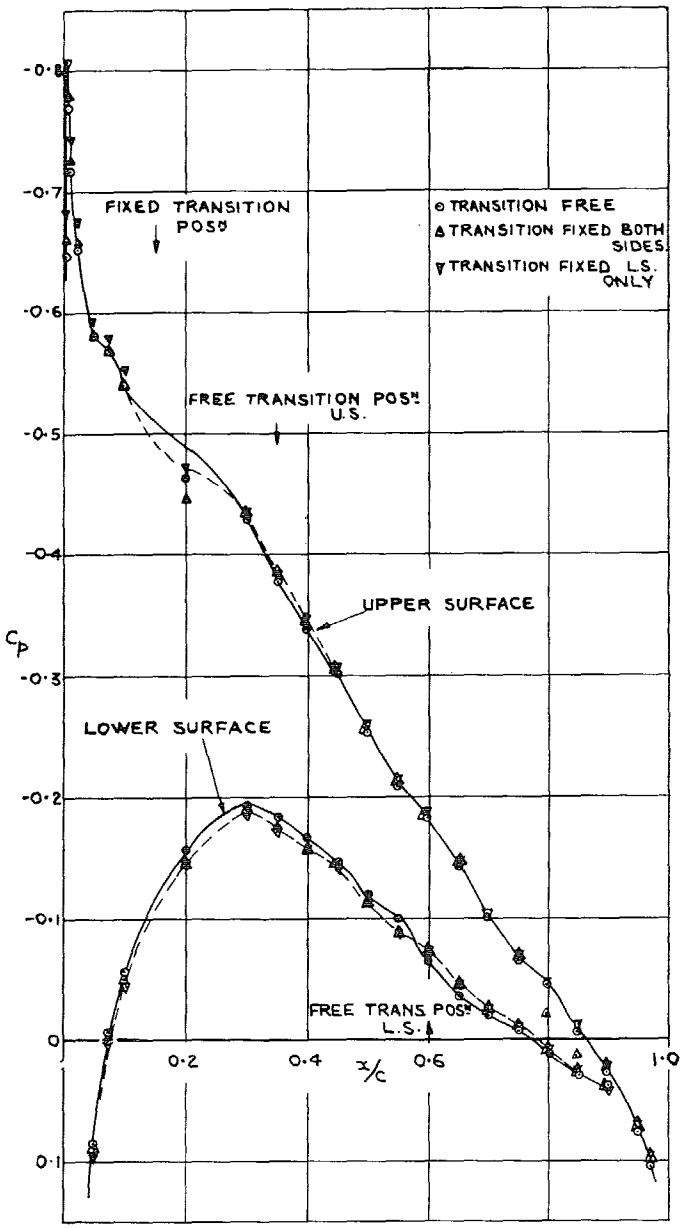

FIG. 7. Effect of fixing transition on the pressure distribution : upper and lower surfaces.
$\alpha \simeq 2$ deg. $R = 3{\cdot}2 \times 10^6$.

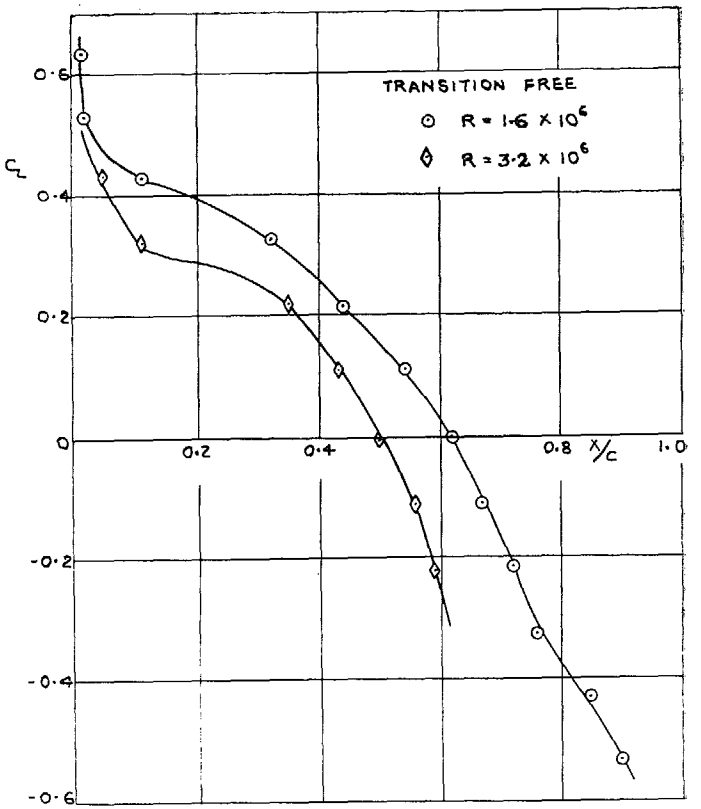

FIG. 8. Position of free transition point.

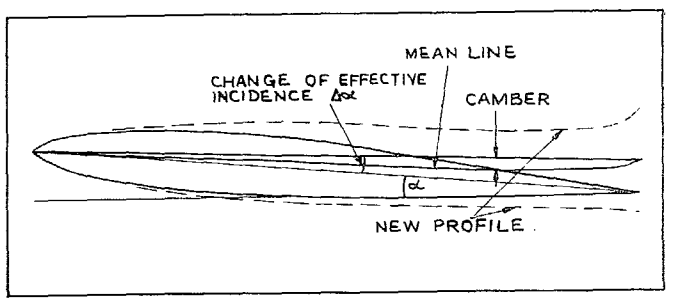

FIG. 9. New profile obtained by adding the displacement thickness.

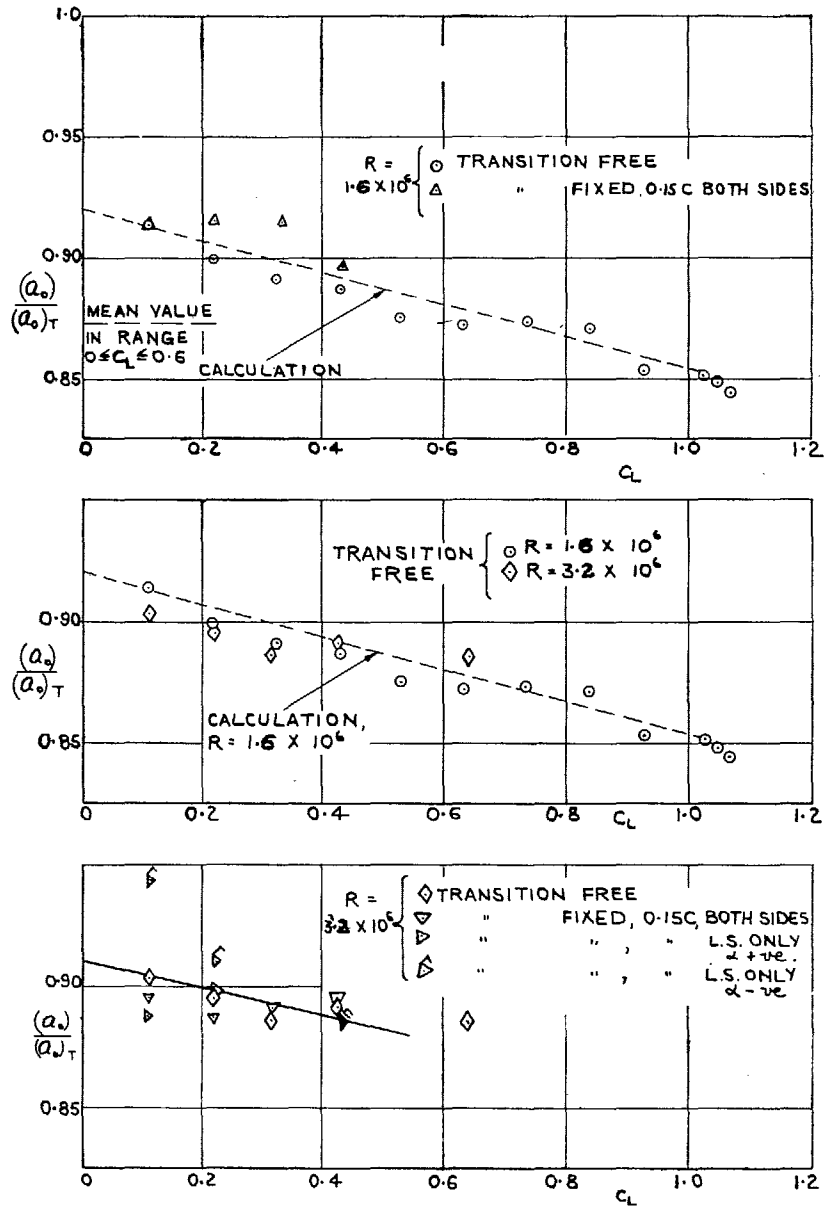

FIG. 10. Two-dimensional lift slopes.

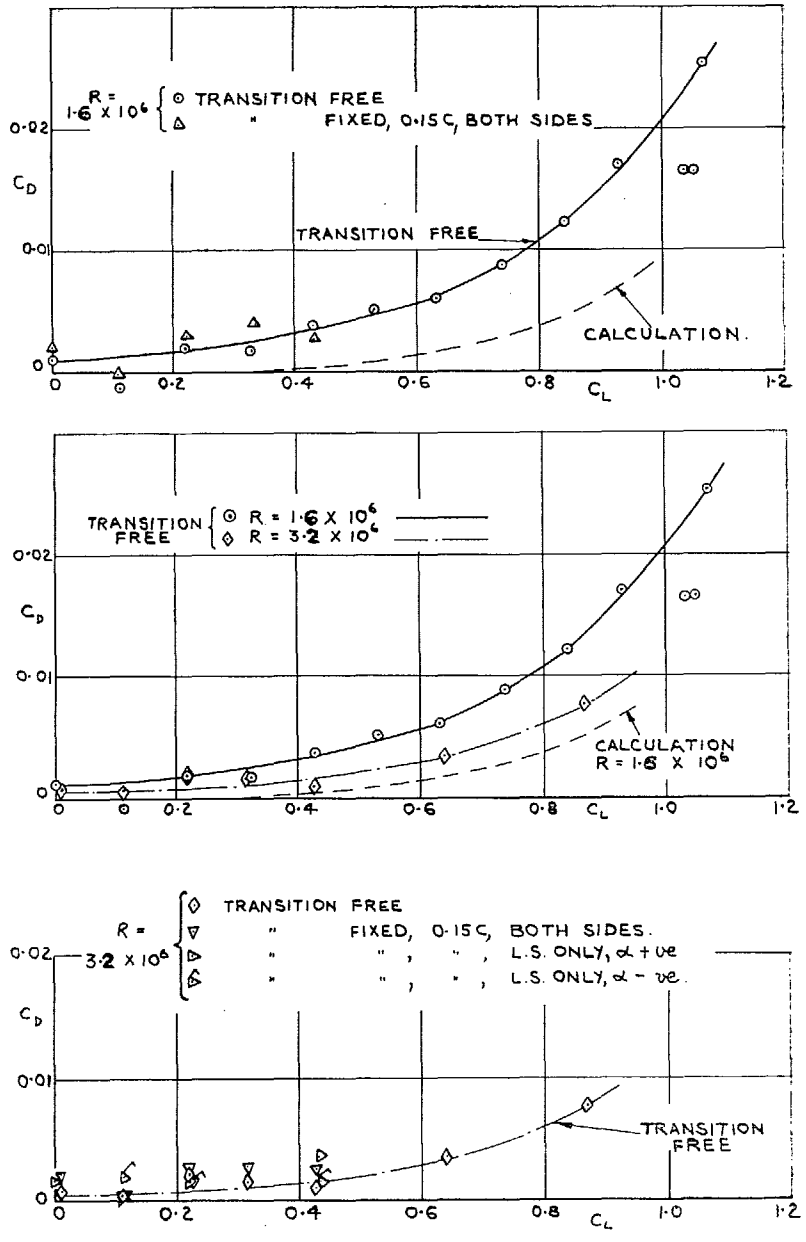

FIG. 11. Two-dimensional form drag.

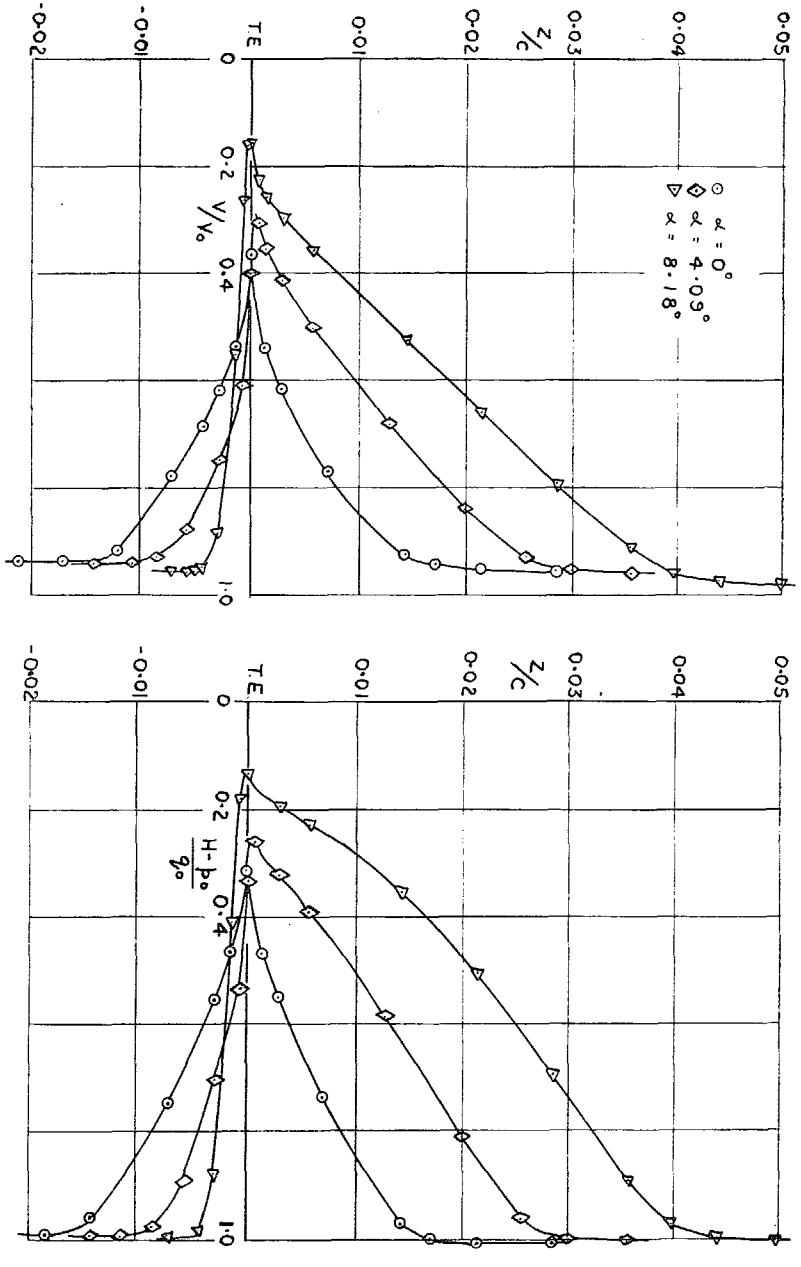

FIG. 13. Velocity and total head at $x/c = 1 \cdot 0015$ (trailing edge).

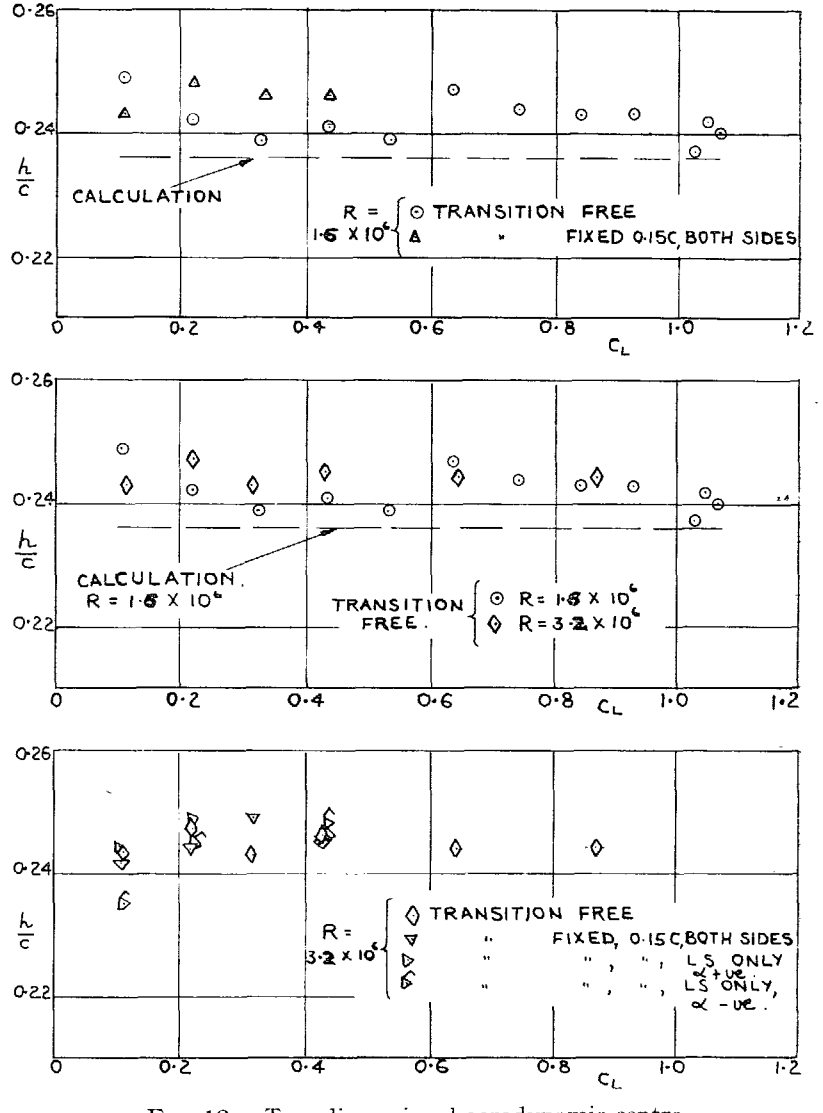

FIG. 12. Two-dimensional aerodynamic centre.

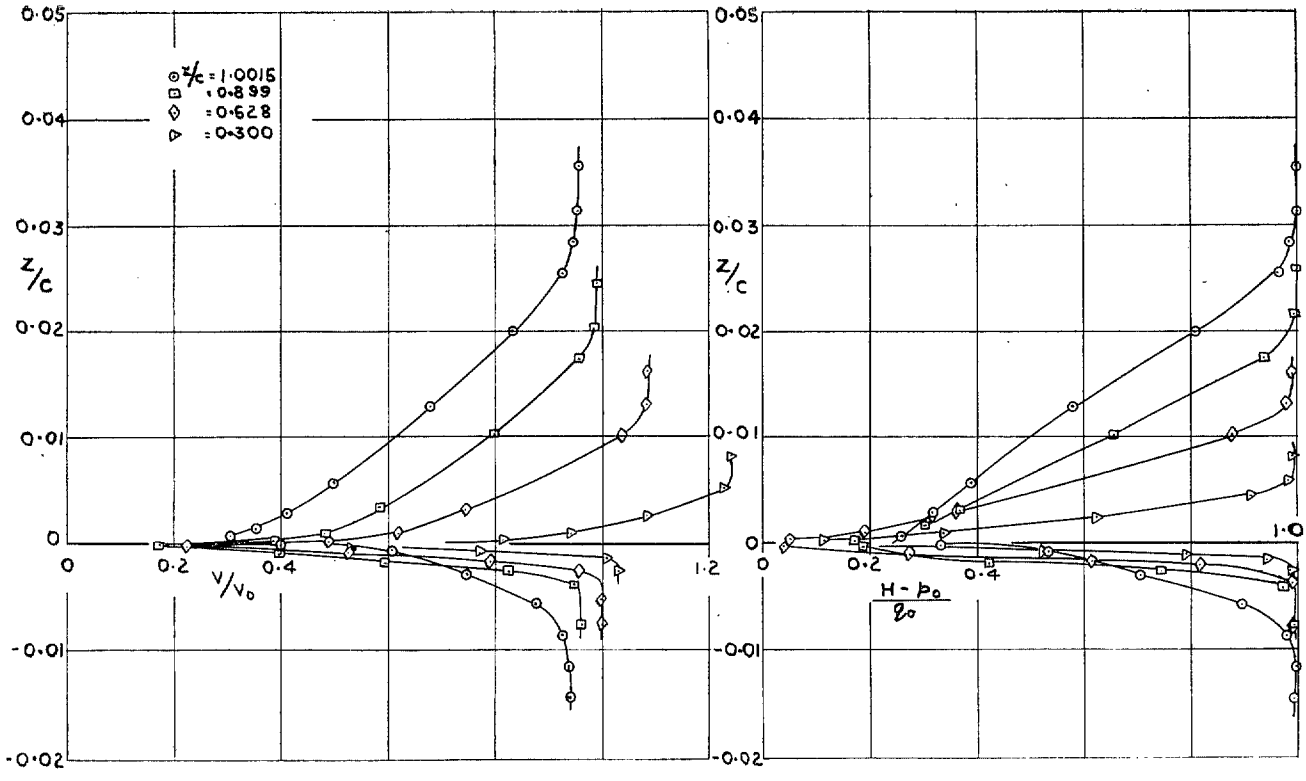

FIG. 14. Velocity and total head at four chordwise positions. $\alpha = 4 \cdot 09$ deg.

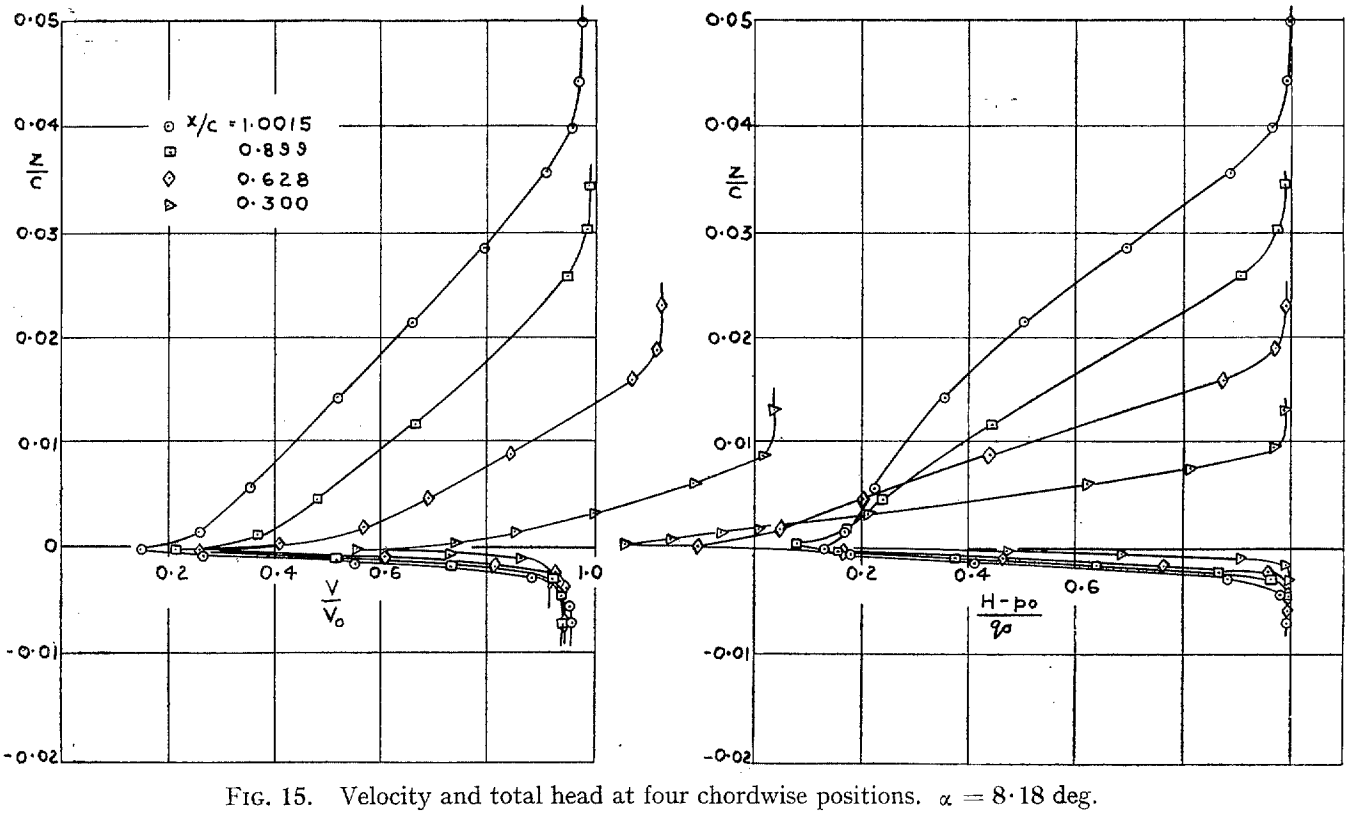

FIG. 15. Velocity and total head at four chordwise positions. $\alpha = 8 \cdot 18$ deg.

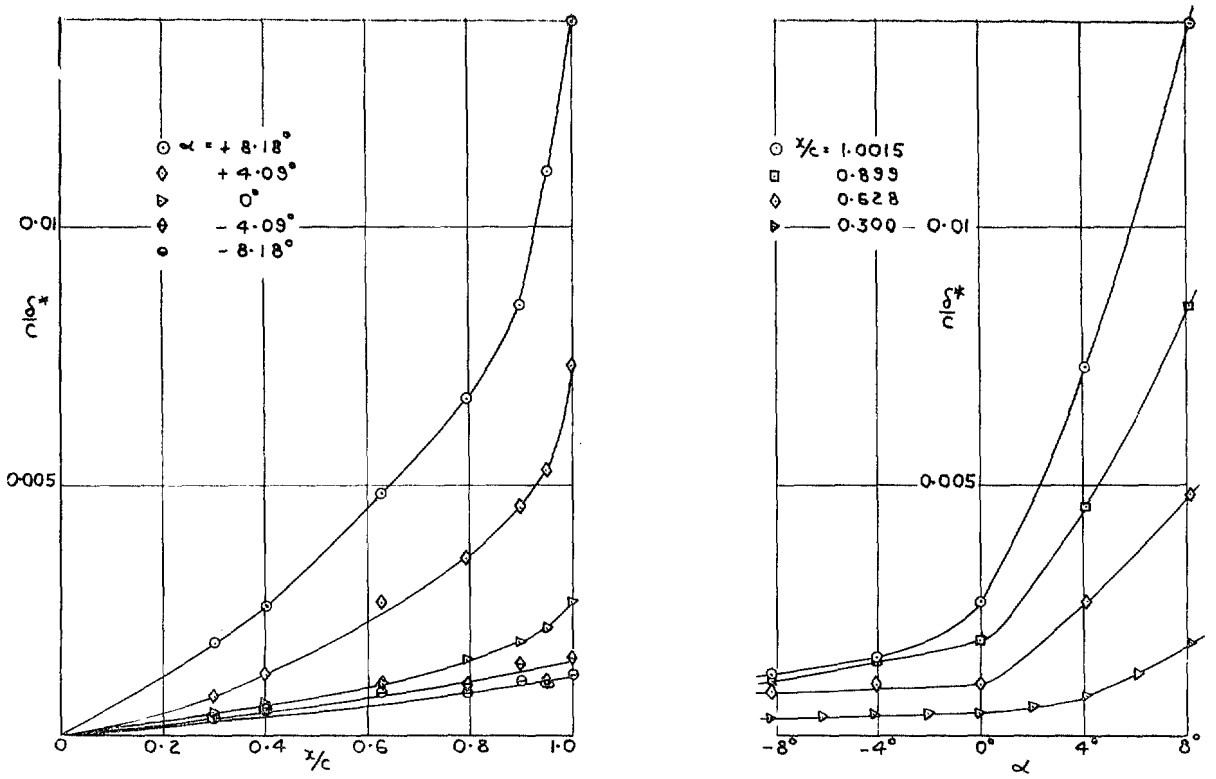

FIG. 16. Displacement thickness.

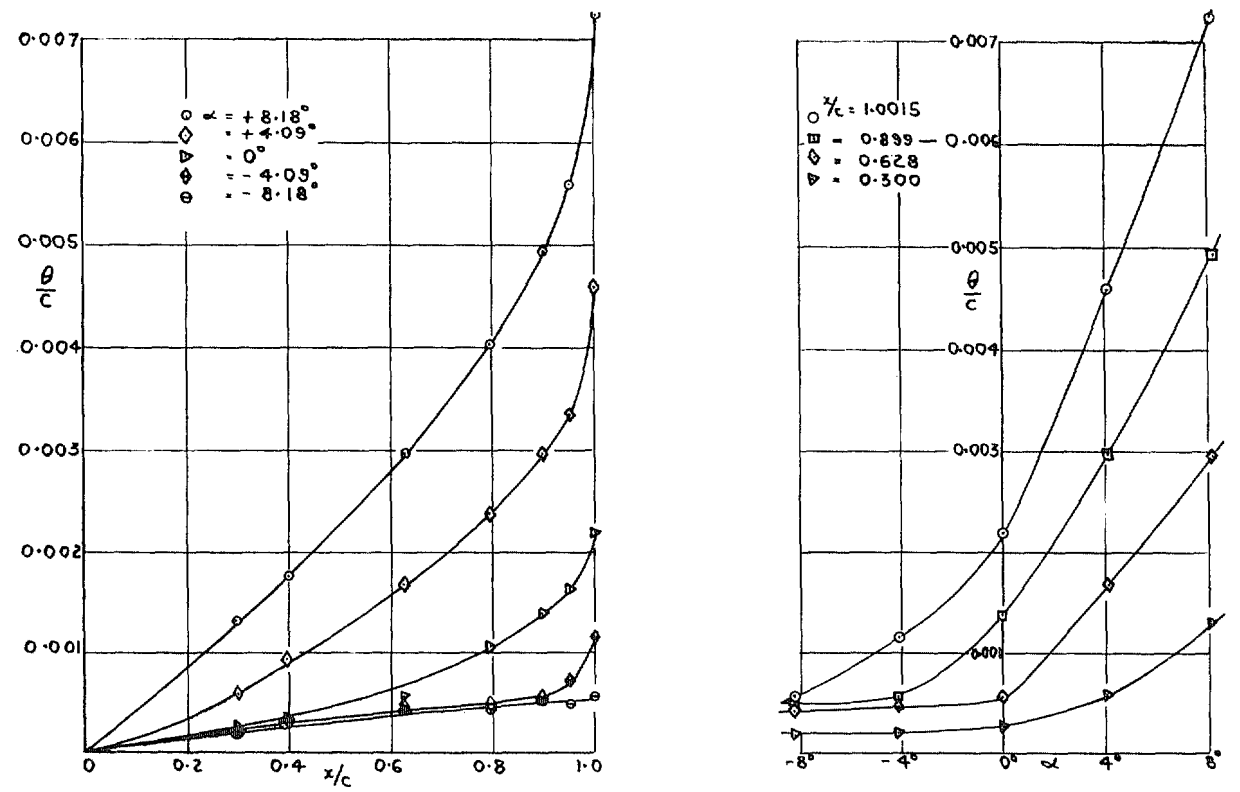

FIG. 17. Momentum thickness.

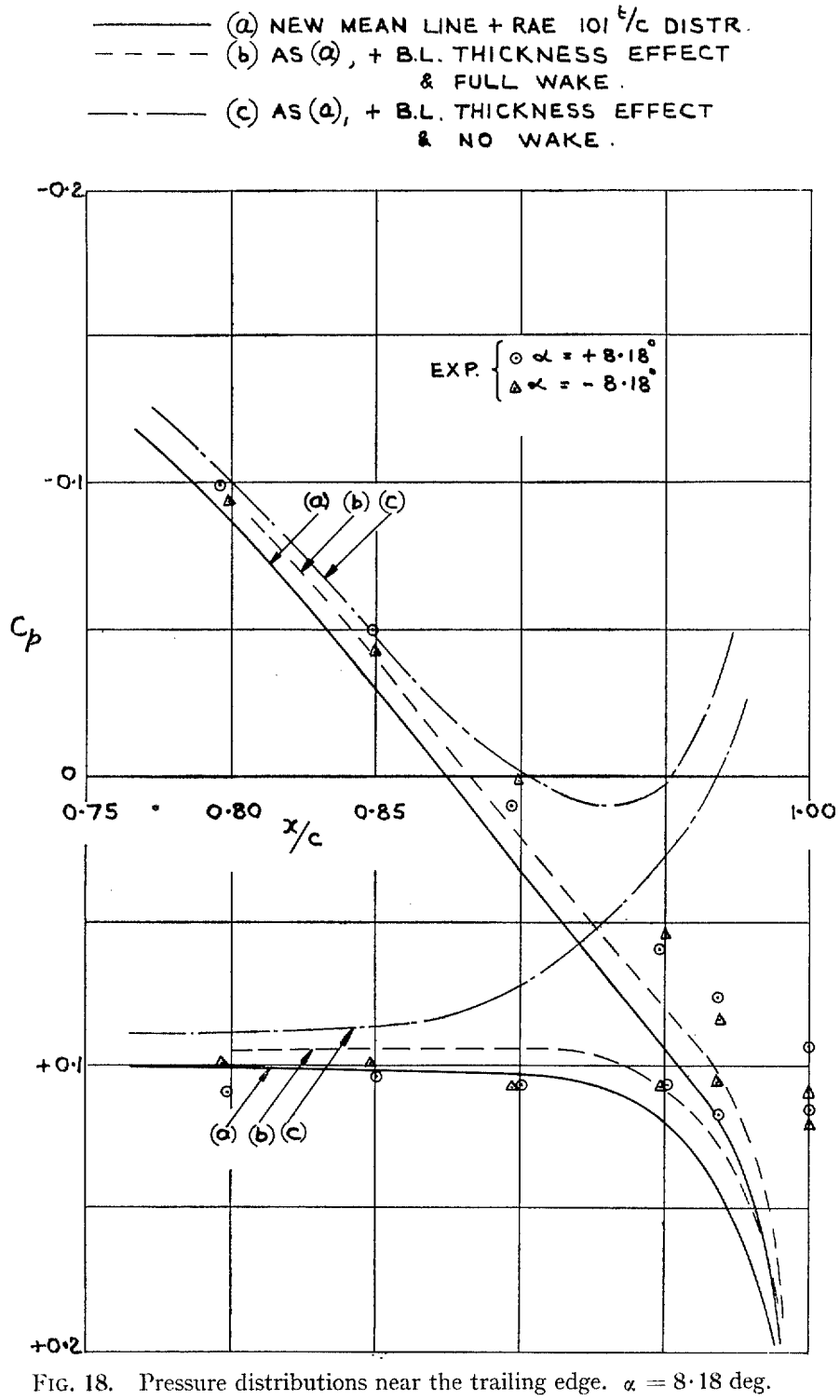

FIG. 18. Pressure distributions near the trailing edge. $\alpha = 8{\cdot}18$ deg.

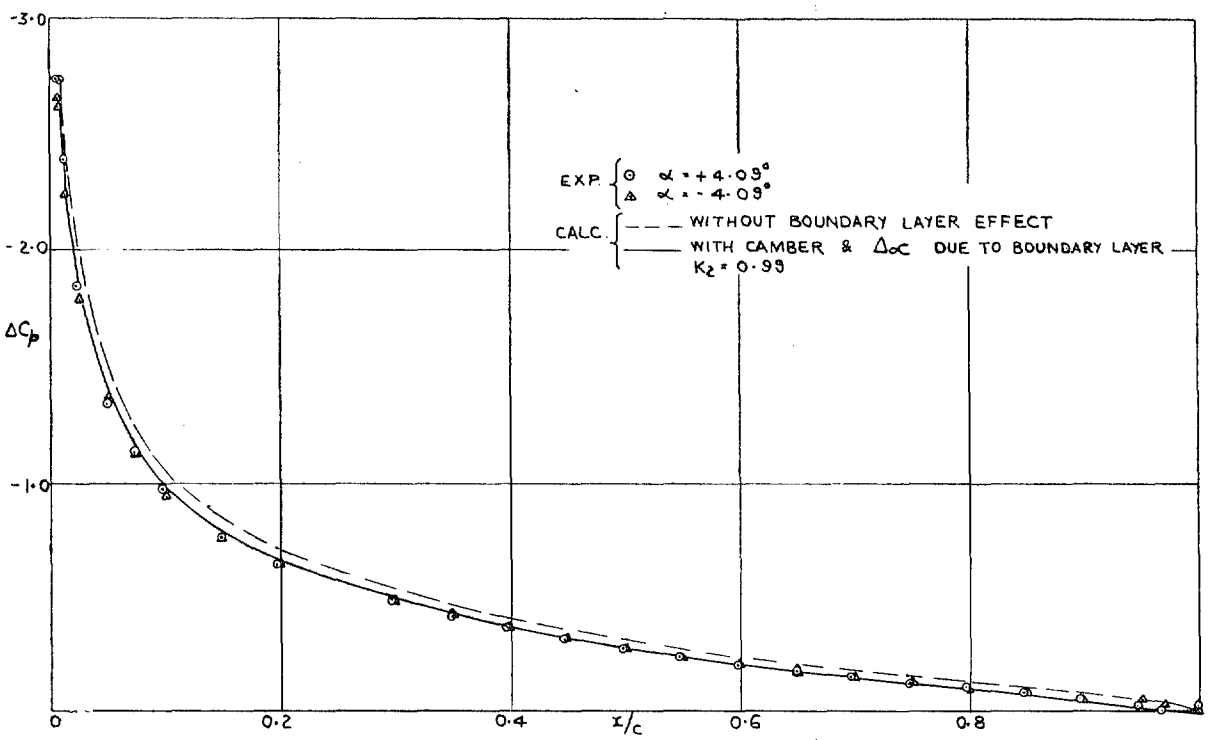

FIG. 19. Experimental and calculated chordwise loading at $\alpha = 4{\cdot}09$ deg, showing effect of boundary layer.

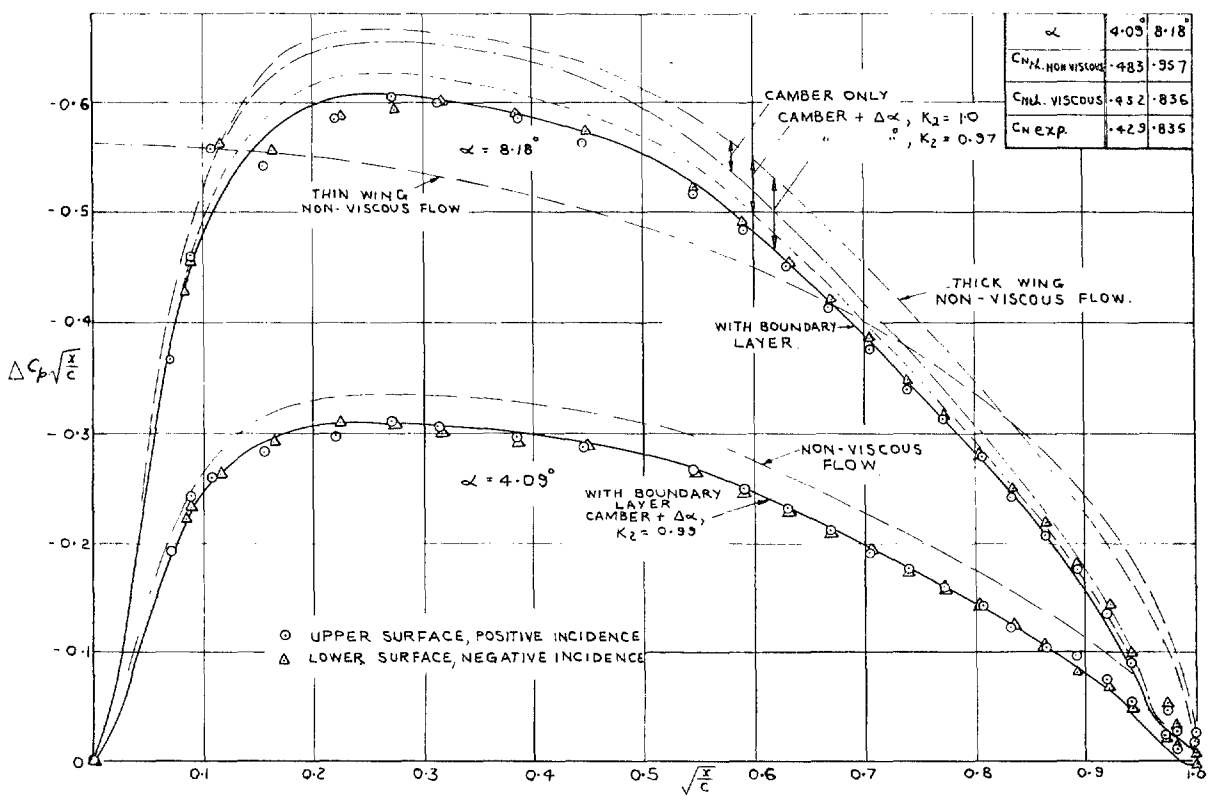

FIG. 20. Experimental and calculated chordwise loading, showing effect of boundary layer.

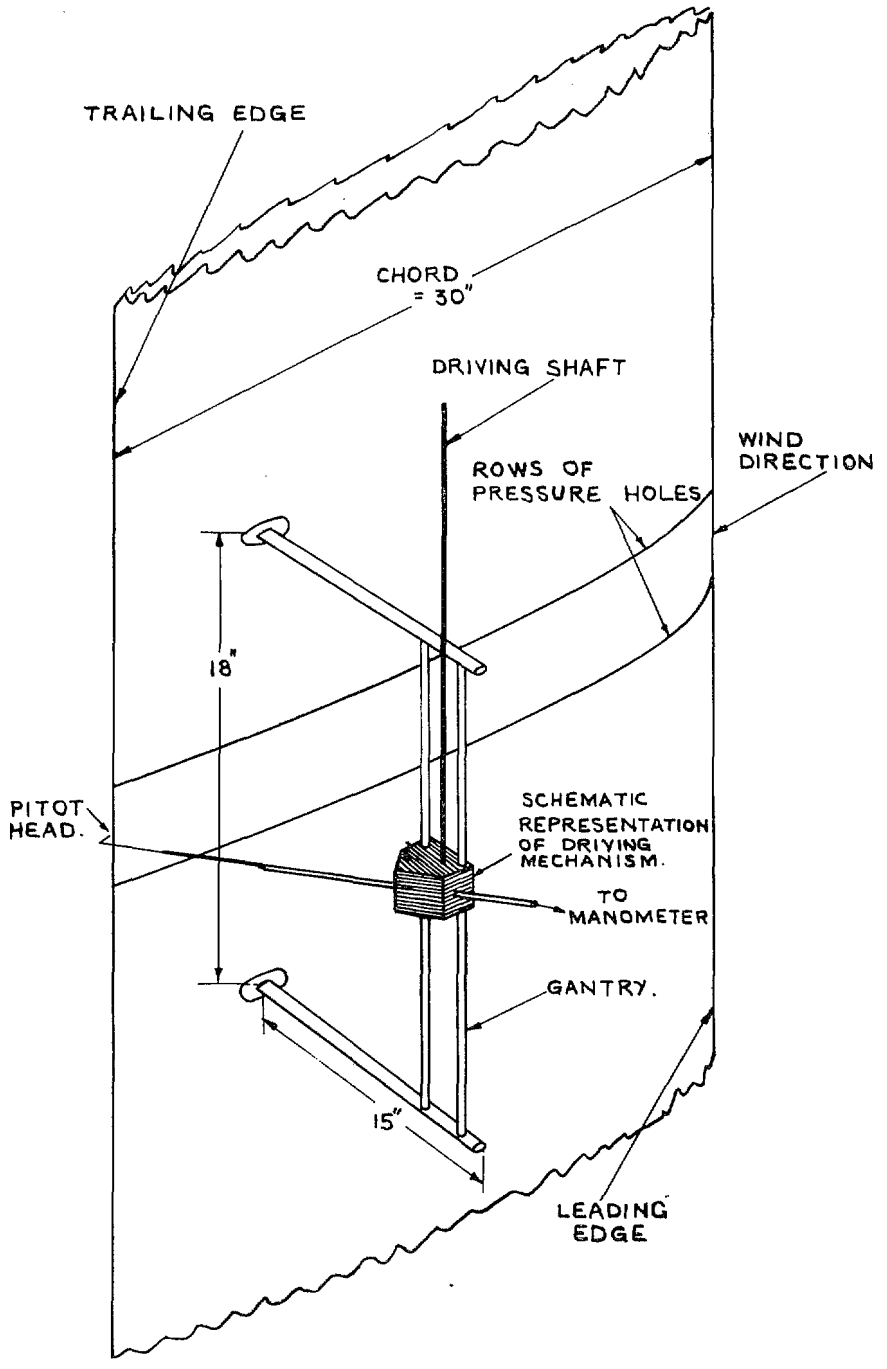

FIG. 21. Sketch of apparatus for measuring the boundary layer.

J4322 Wt.18/9296 K7 2/56 D&Co. 34/263

PRINTED IN GREAT BRITAIN

Publications of the Aeronautical Research Council

ANNUAL TECHNICAL REPORTS OF THE AERONAUTICAL RESEARCH COUNCIL (BOUND VOLUMES)

1938 Vol. I. Aerodynamics General, Performance, Airscrews. 50*s*. (51*s*. 8*d*.)
Vol. II. Stability and Control, Flutter, Structures, Seaplanes, Wind Tunnels, Materials. 30*s*. (31*s*. 8*d*.)

1939 Vol. I. Aerodynamics General, Performance, Airscrews, Engines. 50*s*. (51*s*. 8*d*.)
Vol. II. Stability and Control, Flutter and Vibration, Instruments, Structures, Seaplanes, etc. 63*s*. (64*s*. 8*d*.)

1940 Aero and Hydrodynamics, Aerofoils, Airscrews, Engines, Flutter, Icing, Stability and Control, Structures, and a miscellaneous section. 50*s*. (51*s*. 8*d*.)

1941 Aero and Hydrodynamics, Aerofoils, Airscrews, Engines, Flutter, Stability and Control, Structures. 63*s*. (64*s*. 8*d*.)

1942 Vol. I. Aero and Hydrodynamics, Aerofoils, Airscrews, Engines. 75*s*. (76*s*. 8*d*.)
Vol. II. Noise, Parachutes, Stability and Control, Structures, Vibration, Wind Tunnels. 47*s*. 6*d*. (49*s*. 2*d*.)

1943 Vol. I. Aerodynamics, Aerofoils, Airscrews. 80*s*. (81*s*. 8*d*.)
Vol. II. Engines, Flutter, Materials, Parachutes, Performance, Stability and Control, Structures. 90*s*. (91*s*. 11*d*.)

1944 Vol. I. Aero and Hydrodynamics, Aerofoils, Aircraft, Airscrews, Controls. 84*s*. (86*s*. 9*d*.)
Vol. II. Flutter and Vibration, Materials, Miscellaneous, Navigation, Parachutes, Performance, Plates and Panels, Stability, Structures, Test Equipment, Wind Tunnels. 84*s*. (86*s*. 9*d*.)

ANNUAL REPORTS OF THE AERONAUTICAL RESEARCH COUNCIL—

1933–34	1*s*. 6*d*. (1*s*. 8½*d*.)	1937	2*s*. (2*s*. 2½*d*.)
1934–35	1*s*. 6*d*. (1*s*. 8½*d*.)	1938	1*s*. 6*d*. (1*s*. 8½*d*.)
April 1, 1935 to Dec. 31, 1936	4*s*. (4*s*. 5½*d*.)	1939–48	3*s*. (3*s*. 3½*d*.)

INDEX TO ALL REPORTS AND MEMORANDA PUBLISHED IN THE ANNUAL TECHNICAL REPORTS, AND SEPARATELY—

April, 1950 – – – – – R. & M. No. 2600. 2*s*. 6*d*. (2*s*. 7½*d*.)

AUTHOR INDEX TO ALL REPORTS AND MEMORANDA OF THE AERONAUTICAL RESEARCH COUNCIL—

1909–January, 1954 – – – R. & M. No. 2570. 15*s*. (15*s*. 5½*d*.)

INDEXES TO THE TECHNICAL REPORTS OF THE AERONAUTICAL RESEARCH COUNCIL—

December 1, 1936 — June 30, 1939.	R. & M. No. 1850.	1*s*. 3*d*. (1*s*. 4½*d*.)
July 1, 1939 — June 30, 1945. –	R. & M. No. 1950.	1*s*. (1*s*. 1½*d*.)
July 1, 1945 — June 30, 1946. –	R. & M. No. 2050.	1*s*. (1*s*. 1½*d*.)
July 1, 1946 — December 31, 1946.	R. & M. No. 2150.	1*s*. 3*d*. (1*s*. 4½*d*.)
January 1, 1947 — June 30, 1947. –	R. & M. No. 2250.	1*s*. 3*d*. (1*s*. 4½*d*.)

PUBLISHED REPORTS AND MEMORANDA OF THE AERONAUTICAL RESEARCH COUNCIL—

Between Nos. 2251–2349. – –	R. & M. No. 2350.	1*s*. 9*d*. (1*s*. 10½*d*.)
Between Nos. 2351–2449. – –	R. & M. No. 2450.	2*s*. (2*s*. 1½*d*.)
Between Nos. 2451–2549. – –	R. & M. No. 2550.	2*s*. 6*d*. (2*s*. 7½*d*.)
Between Nos. 2551–2649. – –	R. & M. No. 2650.	2*s*. 6*d*. (2*s*. 7½*d*.)

Prices in brackets include postage

HER MAJESTY'S STATIONERY OFFICE

York House, Kingsway, London W.C.2; 423 Oxford Street, London W.1 (Post Orders: P.O. Box 569, London S.E.1); 13a Castle Street, Edinburgh 2; 39 King Street, Manchester 2; 2 Edmund Street, Birmingham 3; 109 St. Mary Street, Cardiff; Tower Lane, Bristol 1; 80 Chichester Street, Belfast, *or through any bookseller*

S.O. Code No. 23-2886